

# 1 Topological segregation of functional 2 networks increases in developing 3 brains

4 **Wei He<sup>1,2</sup>, Paul F. Sowman<sup>1,2</sup>, Jon Brock<sup>2</sup>, Andrew C. Etchell<sup>2</sup>, Cornelis J. Stam<sup>3</sup>,**  
5 **Arjan Hillebrand<sup>3\*</sup>**

\*For correspondence:  
[wei.he@mq.edu.au](mailto:wei.he@mq.edu.au) (Wei He)

6 <sup>1</sup>Department of Cognitive Science, Macquarie University, 16 University Avenue, Sydney,  
7 Australia; <sup>2</sup>Australian Research Council Centre of Excellence in Cognition and Its  
8 Disorders, 16 University Avenue, Sydney, Australia; <sup>3</sup>Amsterdam UMC, Vrije Universiteit  
9 Amsterdam, Department of Clinical Neurophysiology and MEG Center, Amsterdam  
10 Neuroscience, De Boelelaan 1117, Amsterdam, The Netherlands

---

11  
12 **Abstract** A growing literature conceptualises human brain development from a network  
13 perspective, but it remains unknown how functional brain networks are refined during the  
14 preschool years. The extant literature diverges in its characterisation of functional network  
15 development, with little agreement between haemodynamic- and electrophysiology-based  
16 measures. In children aged from 4 to 12 years, as well as adults, age appropriate  
17 magnetoencephalography was used to estimate unbiased network topology, using minimum  
18 spanning tree (MST) constructed from phase synchrony between beamformer-reconstructed  
19 time-series. During childhood, network topology becomes increasingly segregated, while cortical  
20 regions decrease in centrality. We propose a heuristic MST model, in which a clear developmental  
21 trajectory for the emergence of complex brain networks is delineated. Our results resolve  
22 topological reorganisation of functional networks across temporal and spatial scales in youth and  
23 fill a gap in the literature regarding neurophysiological mechanisms of functional brain maturation  
24 during the preschool years.

---

## 25 **Introduction**

26 Modern network science has revealed that normal brain networks exhibit fundamental properties  
27 of three canonical network extremes - a *random network* (**Erdős and Rényi, 1959**), a locally connected  
28 and highly *ordered (regular) network* (**Mulder, 1992**), and a *scale-free network* with a small number  
29 of highly connected nodes (so-called "hubs", **Barabasi and Albert 1999**). Adult brain networks also  
30 display hierarchical modularity (**Meunier et al., 2009; Stam, 2014; Wig, 2017**), in which modules that  
31 include regions from the default mode, fronto-parietal, parieto-temporal, or subcortical networks  
32 support specific cognitive functions (**Bullmore et al., 2009; Fornito et al., 2011; Power et al., 2011**).  
33 A heuristic model of complex brain networks has been proposed (**Stam and van Straaten, 2012**) to  
34 characterise the properties of real brain networks in an abstract "network space" defined by the  
35 four network models (i.e., regular, random, scale-free, and hierarchical modular networks). This  
36 heuristic model of "network space" suggests that the hierarchical modular network is an "attractor"  
37 for healthy brain networks and the other three extreme networks are "attractors" for different  
38 stages or patterns of brain diseases (**Stam and van Straaten, 2012; Stam, 2014**).

39 Despite the robust and reproducible description of adult brain networks, there is relatively  
40

41 scant data regarding the maturation of brain networks. Such data can be acquired non-invasively  
42 using magnetic resonance imaging (MRI) or electrophysiological techniques (such as magnetoen-  
43 cephalography/MEG and electroencephalography/EEG). Studies using MRI-based measurements  
44 have demonstrated that both functional and structural brain networks become more segregated  
45 during childhood (e.g., functional MRI: *Fair et al. 2009*; *Gu et al. 2015*; *Supekar et al. 2009*; structural  
46 MRI: *Huang et al. 2015*; and diffusion-weighted imaging: *Baum et al. 2017*). Such development  
47 allows for an ongoing balance between the *integration* of converging information from distributed  
48 brain regions, and at the same time the *segregation* of divergent specialised information streams  
49 (*Fair et al., 2009*; *Grayson and Fair, 2017*; *Richmond et al., 2016*; *Rubinov and Sporns, 2010*). How-  
50 ever, most studies to date have only focused on children older than 6 years or younger than 3 years  
51 of age (*Grayson and Fair, 2017*), leaving the preschool years of childhood (between 3 and 6 years of  
52 age) understudied – a knowledge gap that has been termed “the missing neurobiology of cognitive  
53 development” (*Poldrack, 2010*).

54 Furthermore, there is little agreement between MRI- and electrophysiology-based network de-  
55 scriptions. Correspondence between functional MRI and electrophysiological measures of functional  
56 brain networks (*Brookes et al., 2011*) implies that changes in functional MRI network organisation  
57 should be, at least partially, preserved in higher temporally-resolved electrophysiological investi-  
58 gations (*Grayson and Fair, 2017*). It follows then, that electrophysiological networks are expected  
59 to become increasingly segregated during childhood development. However, prior EEG studies  
60 have reported conflicting results, which include increasing segregation (*Boersma et al., 2011, 2013*;  
61 *Janssen et al., 2017*; *Toth et al., 2017*), decreasing segregation (*Smit et al., 2016*; *Bathelt et al., 2013*;  
62 *Miskovic et al., 2015*), or no changes with age (*Schafer et al., 2014*). Discrepancy between develop-  
63 mental MRI- and electrophysiology-based network findings has been difficult to reconcile, partly  
64 due to the different spatial scales that functional networks have been examined at (sensor-level  
65 in most EEG versus cortical-level in fMRI studies). Modern whole-head magnetoencephalography  
66 (MEG) allows for sophisticated spatial filtering techniques to accurately (varying from sub-millimetre  
67 to a few centimetres) reconstruct millisecond electrophysiological time series across the cortex  
68 (*Hillebrand et al., 2005*; *Troeinger et al., 2014*; *Barratt et al., 2018*), and thus MEG is a critical tool  
69 in the quest to resolve these discrepancies.

70 To better understand how the topology of functional brain networks develops over the whole  
71 period of childhood, we used MEG to collect resting-state electrophysiological signals from children  
72 whose ages spanned 4 to 12 years, as well as from adults. Importantly, we utilised a paediatric  
73 MEG system with a child-sized helmet for data collection in children aged under 6 years (*He et al.,*  
74 *2014*; *Johnson et al., 2010*). We hypothesised that, based on the heuristic model of complex brain  
75 networks, the healthy brain develops from a more random and integrated structure towards a  
76 configuration that offers a balance between network integration and segregation during norma-  
77 tive development (*Stam, 2014*). Specifically, we predicted that: (1) functional networks become  
78 more segregated, shifting from a centralised network topology to a de-centralised configuration  
79 (*Boersma et al., 2013*; *Toth et al., 2017*); (2) individual brain regions become more diverse in their  
80 connectedness, i.e., centrality of brain regions increases for hubs (e.g., regions in the default mode  
81 and the fronto-parietal areas), but decreases in non-hub regions (e.g., regions in the primary visual  
82 and auditory areas).

## 83 Results

84 We applied an atlas-based beamforming approach (*Hillebrand et al., 2012*) to reconstruct time  
85 series of neuronal activity recorded using a child-customised 125-channel whole-head gradiometer  
86 MEG system optimised for children aged around 5 years (5 year-olds (Y.O.),  $N = 10$ ,  $5.4 \pm 1.1$  years, 5  
87 males). We used a 160-channel whole-head gradiometer MEG system for children aged around 10  
88 years (10 year-olds (Y.O.),  $N = 14$ ,  $9.8 \pm 1.5$  years, 12 males) and adults ( $N = 24$ ,  $40.6 \pm 17.4$  years,  
89 16 males). Functional connectivity between the 80 regions of interest (ROIs; 78 cortical ROIs and  
90 bilateral hippocampi) in the automated anatomical labelling (AAL; *Tzourio-Mazoyer et al. 2002*) atlas

91 was estimated using the phase lag index (PLI). Averaged PLI was computed between a region and  
92 all 79 other regions, resulting in a single estimation of functional connectivity per participant. There  
93 were no significant PLI differences between the three age groups for any of the 5 frequency bands  
94 (delta: 0.5–4 Hz, theta: 4–8 Hz, alpha: 8–13 Hz, beta: 13–30 Hz, and low gamma: 30–48 Hz).

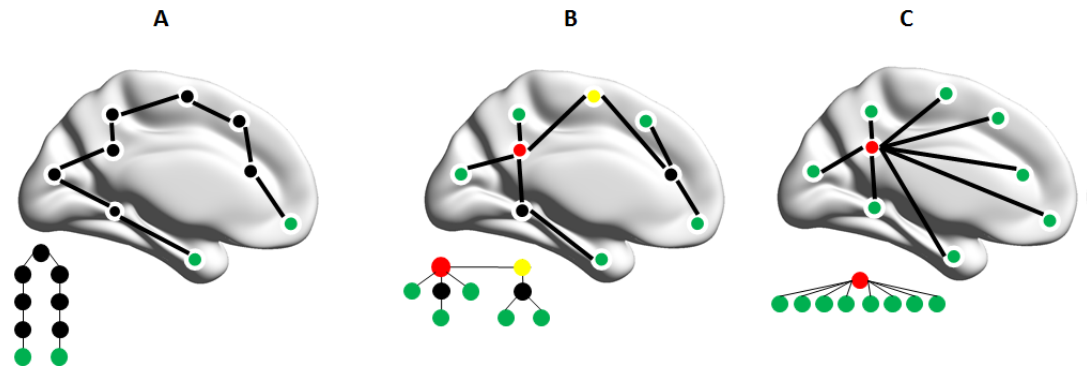


**Figure 1.** Minimum spanning tree (MST) topology and hierarchy of three representative tree models. Top panel: (A) a line-like tree, and (C) a star-like tree. (B) an intermediate configuration between the two extremes. Nodes are indicated by circles, and links by connecting lines. Green nodes are leaves, which have a **Degree** (i.e., number of links to neighbouring nodes) of 1; red nodes are hubs that have the highest **Degree** and **Betweenness Centrality** (i.e., the fraction of the smallest number of links between any two nodes in a network that pass through a node); the yellow node and the red node in B, have the lowest **Eccentricity** (i.e., the largest number of links required for a node reaching any other node in a network). The **Diameter** in B is 5 (i.e., the longest distance between any two nodes in a network). The three lower graphs are the same trees as those overlaid on the template brains above but represented in a way that illustrates that trees with more leaves have fewer layers (nodes with the lowest **Eccentricity** are placed on top). Network A requires many steps for an individual node, especially a leaf node in green, to connect to other nodes (low *integration* and high *segregation*). The steps required for nodes to connect with each other are fewer in C but the central hub/red node is considered 'overloaded' (high *integration* but low *segregation*). The network between these extremes - network B - represents a hierarchical tree, which offers a balance between information *integration* and *segregation*.

95 Subsequently, we reconstructed the minimum spanning tree (MST; **Figure 1**; **Kruskal 1956**; **Wang**  
96 **et al. 2008**), so that the topology of functional networks could be characterised and compared  
97 without biases that are inherent in conventional graph theoretical approaches (**Stam, 2014**; **Tewarie**  
98 **et al., 2015**). The MST is a sub-network that contains the strongest connections within a weighted  
99 network without forming cycles or loops; it provides an unbiased reconstruction of the core of a  
100 network, making it possible to create a unique backbone or empirical reference network (e.g., for  
101 large datasets such as the human brain connectome project; **van Dellen et al. 2018**). Moreover,  
102 MST parameters are sensitive to alterations in the topology of brain networks at the functional- (e.g.,  
103 **Boersma et al. 2013**; **de Bie et al. 2012**; **Janssen et al. 2017**) and structural-level (e.g., **Otte et al.**  
104 **2015**; **van Dellen et al. 2018**), and importantly, can be interpreted along the lines of conventional  
105 graph theoretical measures (**Tewarie et al., 2016**).

### 106 **Topological segregation of the large-scale functional networks**

107 We first sought to understand whether the topology of the functional networks become more  
108 segregated during childhood development. To this end, we calculated 5 global MST measures for  
109 each participant: Diameter, Leaf Fraction, Tree Hierarchy, Degree Correlation, and Kappa. Small  
110 Diameter and high Leaf Fraction are characteristic for a highly integrated topology such as a star-like  
111 network (A in **Figure 1**), whereas large Diameter and low Leaf Fraction are representative of a more  
112 segregated topology or line-like network (C in **Figure 1**). An optimal MST topology, requiring a small  
113 Diameter without overloading central nodes, is quantified by Tree Hierarchy (**Boersma et al., 2013**;  
114 **Tewarie et al., 2015**). Such a network topology also tends to have larger Degree Correlation and  
115 Kappa, suggesting it is resilient against random damage (**Barrat et al., 2008**; **Van Mieghem et al.,**

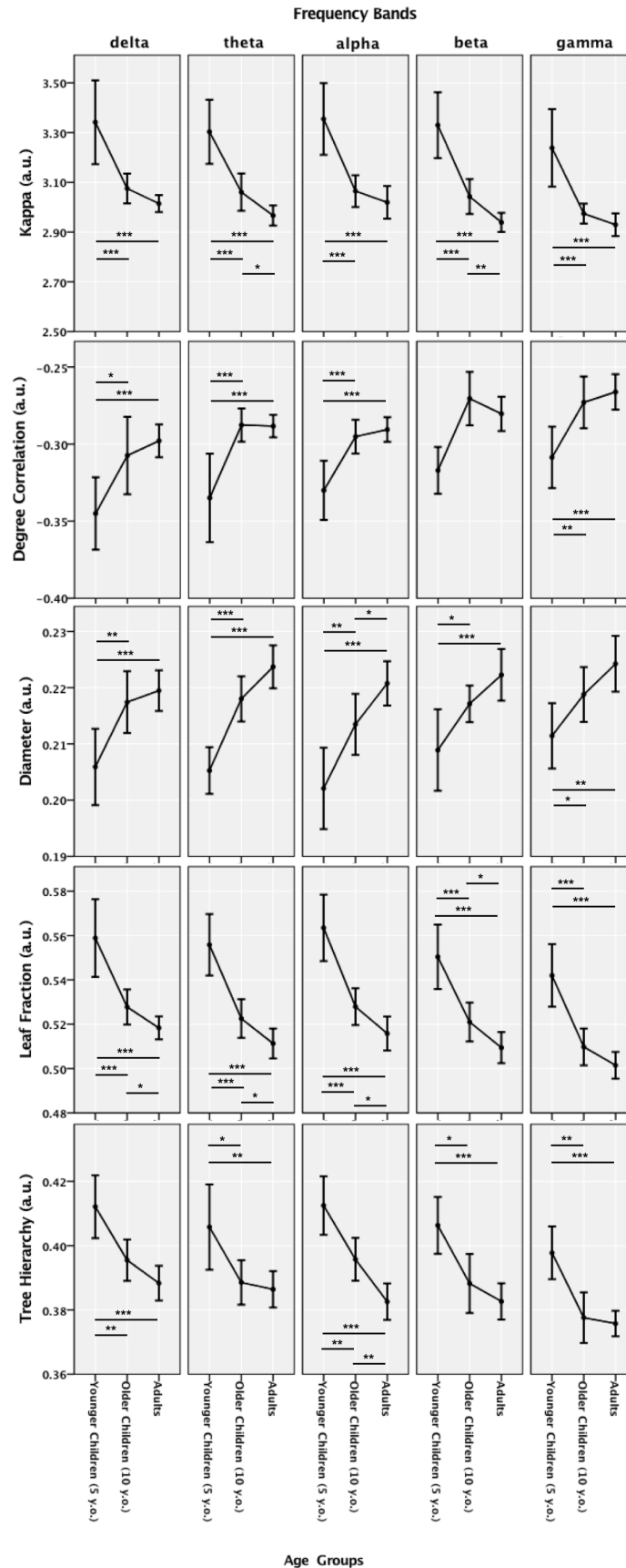


**Figure 2.** Minimum spanning tree (MST) global metrics estimated from individual phase lag index adjacency matrices in the delta (0.5–4 Hz), theta (4–8 Hz), alpha (8–13 Hz), beta (13–30 Hz), and low gamma (30–48 Hz) bands for three age groups (5 year-olds (Y.O.), 10 year-olds (Y.O.), and Adults). Error bars depict 95% confidence intervals estimated using bootstrapping with 1000 random iterations. \* indicates statistically significant group differences ( $p < 0.05$ , 50000 random permutations), \*\* for  $p < 0.01$ , and \*\*\* for  $p < 0.001$ .

116 **2010).**

117 The 5 global MST measures were significantly different across all 5 frequency bands  
118 when comparing children (as a whole group)  
119 to adults: Kappa, Leaf Fraction, and Tree Hier-  
120 archy were higher, whereas Degree Correla-  
121 tion and Diameter were lower, in the children  
122 (**Figure 2**). These frequency-independent effects  
123 were all highly significant ( $p < 0.001$ )  
124 when contrasting 5 Y.O. with the other two  
125 age groups, but less so when comparing 10  
126 Y.O. with adults. The 10 Y.O. was adult like  
127 for most global MST topological measures,  
128 apart from larger Leaf Fraction in the delta  
129 ( $p = 0.036$ ) and beta ( $p = 0.041$ ) bands, larger  
130 Kappa ( $p = 0.017$ ) and Leaf Fraction ( $p = 0.036$ )  
131 in the theta band, and smaller Diameter ( $p$   
132  $= 0.023$ ) but larger Leaf Fraction ( $p = 0.038$ )  
133 and Tree Hierarchy ( $p = 0.007$ ) in the alpha  
134 band. Overall, the MST topology becomes  
135 more line-like and segregated across all fre-  
136 quency bands with increasing age (**Figure 3**).  
137

### 138 **Regional de-centralisation correlates** 139 **with increasing topological segrega-** 140 **tion**

141 Having established that the network topology  
142 is more segregated in adults than in children,  
143 we next investigated the centrality of brain re-  
144 gions. We calculated 3 nodal MST measures  
145 for each of the 80 regions in every participant:  
146 Degree, Betweenness Centrality, and Eccen-  
147 tricity. Larger Degree and Betweenness Cen-  
148 trality, but smaller Eccentricity characterise  
149 regions (or so-called “hubs”) that play a cen-  
150 tral role in the network. We found that, even  
151 though there were no significant group dif-  
152 ferences for the Degree and Betweenness  
153 Centrality, the Eccentricity showed significant  
154 increases from children (as a whole group) to  
155 adults, and from 5 Y.O. to adults in particular.  
156 The group differences for the Eccentricity, il-  
157 lustrated in **Figure 4**, show pervasive changes  
158 in Eccentricity over the cortex (the full results  
159 are shown in Tables 1-5 in **Appendix 1**).

160 When contrasting adults and 5 Y.O.:

- 161 • all 80 ROIs showed larger theta band Eccentricity in adults;
- 162 • in alpha, beta, and delta mediated MSTs, most of the nodes showing larger Eccentricity were  
163 in fronto-parietal areas, followed by the nodes normally assigned to the default mode and  
164 parieto-temporal areas, and in hippocampal and occipital areas;

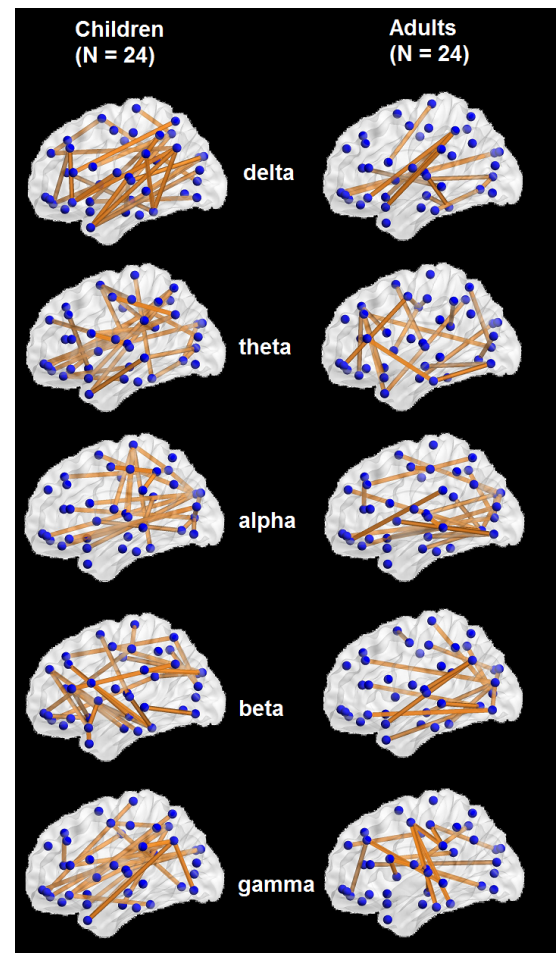


**Figure 3.** Minimum spanning trees (MSTs) for adults ( $N = 24$ ) and children ( $N = 24$ ) in five frequency bands (delta: 0.5–4 Hz, theta: 4–8 Hz, alpha: 8–13 Hz, beta: 13–30 Hz, and low gamma: 30–48 Hz), displayed on a template brain with blue dots depicting nodes and yellow lines depicting functional connections. The MSTs depicted are estimated from averaged phase lag index adjacency matrices from adults (right panel) and children (left panel) for illustrative purposes only. The alpha-mediated MST in adults has fewer leaves and a more line-like topology (with central nodes in occipital regions) than the MST in children. This observation agrees with the statistical comparisons between age groups when the MST metrics were based on the un-averaged adjacency matrices in **Figure 2**.



165 • about half of the nodes in the default mode, parieto-temporal, and the occipital areas showed  
166 larger Eccentricity in gamma mediated MSTs.

167 When comparing adults and 10 Y.O.:

- 168 • most of the nodes showing larger Eccentricity were in the default mode, occipital, parieto-  
169 tempo-  
170 ral, and fronto-parietal areas in alpha band mediated MSTs;
- 170 • nodes from the default mode, parieto-temporal and occipital areas showed larger Eccentricity  
171 in the theta mediated MSTs;
- 172 • nodes from the fronto-parietal, parieto-temporal, and hippocampal areas, as well as the  
173 nodes from the default mode, showed larger Eccentricity in the beta mediated MSTs;
- 174 • only nodes from occipital area and the default mode area showed larger Eccentricity in the  
175 gamma mediated MSTs;
- 176 • no Eccentricity differences were found in the delta mediated MSTs.

177 When contrasting adults to children (as a whole group), and 5 Y.O. to the other two age groups,  
178 the group differences in Eccentricity exhibited a similar pattern, namely that a larger Eccentricity  
179 was found mostly in nodes from the fronto-parietal area, followed by those from default mode,  
180 parieto-temporal, occipital and hippocampal areas in delta-to-gamma mediated MSTs.

## 181 Discussion

182 Capitalising on several novel approaches, we demonstrate in this cross-sectional MEG study that  
183 the topology of functional brain networks becomes segregated during childhood development.  
184 Increasing topological segregation is associated with increasing regional Eccentricity across the  
185 cortex, indicating that most brain regions become functionally specialised and less central in  
186 the network. Specifically, the reorganisation of network topology has the same profile across all  
187 frequency bands and is not routed via a few hub regions. Importantly, all topological network  
188 differences are highly significant between the preschool children/5 Y.O. and older age groups  
189 (i.e., older children/10 Y.O. and adults), suggesting that the preschool years present a unique  
190 and important period of network maturation. These converging results on topological network  
191 changes inform a heuristic MST model from which normal development during childhood can be  
192 characterised.

193 The delineation of large-scale functional brain networks in adults has confirmed a number  
194 of hypotheses regarding the degradation of network function in aging and disease (*Stam, 2014*).  
195 However, the small number of developmental studies that have examined electrophysiological  
196 networks have produced heterogeneous results. Furthermore, these results do not align well with  
197 MRI-based haemodynamic imaging data. Critically, we resolved these discrepancies by utilising  
198 several technical and methodological advances: (1) age-appropriate MEG systems that are insensi-  
199 tive to age-related physiological and anatomical changes in biological tissues (e.g., bone thickness  
200 and density of the skull; *Smith et al. 2012*); (2) source-level functional connectivity estimation to  
201 facilitate interpretation of our results in an anatomical context, and to effectively mitigate spurious  
202 connectivity/network results inherent in sensor-level analyses (*Antiqueira et al., 2010; Lai et al.,*  
203 *2017*); (3) leakage insensitive connectivity estimation using PLI, which effectively ignores spurious  
204 connectivity due to field spread (*Dominguez et al., 2007*) and volume conduction/signal leakage  
205 (*Lai et al., 2017; Schoffelen and Gross, 2009; Stam et al., 2007*); (4) lastly, MST for unbiased network  
206 comparisons between different age groups (*Tewarie et al., 2015; Van Mieghem et al., 2010*).

207 Leveraging data across multiple frequency bands in anatomical space, we demonstrate that  
208 the topology of electrophysiological networks becomes increasingly segregated during childhood,  
209 in line with MRI-based findings (*Baum et al., 2017; Fair et al., 2009; Gu et al., 2015; Huang et al.,*  
210 *2015*). The smaller Diameter and larger Leaf Fraction in children compared to adults indicates  
211 that the topology of the functional brain networks becomes segregated via a transition from a  
212 star-like (centralised) configuration toward a more line-like (de-centralised) configuration during

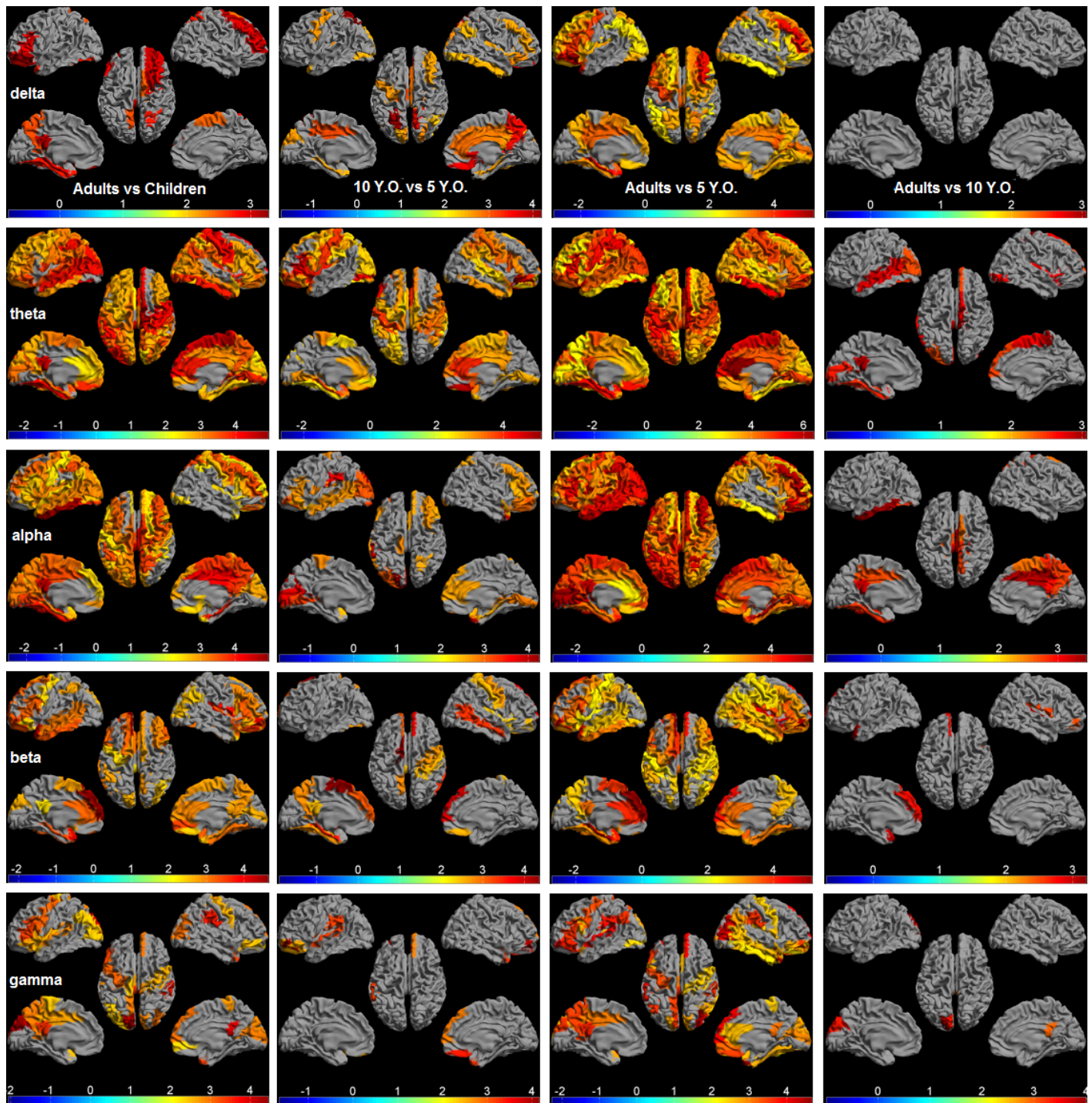


**Figure 4.** Significant differences in the minimum spanning tree (MST) Eccentricity displayed as a color-coded map on the parcellated template brain, viewed from, in clockwise order, the left, top, right, right midline, and left midline. From left to right, pairwise differences (t-value,  $p < 0.05$ , FDR-corrected for 3 nodal MST measures  $\times$  80 ROIs) between adults and children, 10 Y.O. and 5 Y.O., adults and 5 Y.O., as well as adults and 10 Y.O., are shown for all five frequency bands (delta: 0.5–4 Hz, theta: 4–8 Hz, alpha: 8–13 Hz, beta: 13–30 Hz, and low gamma: 30–48 Hz).

213 development. Such network topological change has been found in infants right after birth (*Toth*  
214 *et al., 2017*) and continues up to 18 years of age (*Boersma et al., 2011*). In addition, the observed  
215 larger Kappa in children compared to adults suggests a movement away from a scale-free network.  
216 This finding seems to be at odds with findings from most adult studies, which indicate that the  
217 mature brain network is approximately “scale-free” (*Sporns, 2013*). However, Kappa is not strictly  
218 tied to “scale-freeness”, but rather is a measure for the homogeneity of the degree distribution in  
219 the MST (especially in the case of small networks; *Jinhui et al. 2009*). Moreover, scale-freeness is a  
220 relative measure, and depends on the reference model that the experimental model is compared  
221 to (*Stam and van Straaten, 2012*). Thus, the adult brain may still be scale-free, although less so  
222 than brain networks in children. In accordance with the decreased scale-freeness of adult networks,  
223 the increase in Eccentricity found in a distributed set of brain regions across all frequency bands  
224 suggests that during development most brain regions, including hubs become less central, in order  
225 to prevent hub overloading, as well as to reduce vulnerability to targeted attacks (*Stam et al., 2009*).  
226 Together, decreasing nodal centrality possibly reflects a protective mechanism during normative  
227 brain development, since disturbances and insults to hub regions can produce lifelong changes  
228 in neurological and mental functioning (*Crossley et al., 2014; DeSalvo et al., 2014; Stam et al.,*  
229 *2009; Tewarie et al., 2014; Yu et al., 2017*). Lastly, the smaller Tree Hierarchy found in adults is  
230 less straightforward to understand here, as a decrease in network hierarchy is often observed in  
231 clinical groups (*Stam and van Straaten, 2012*). Tree Hierarchy is a composite MST measure that  
232 takes into account several aspects of the MST, namely the maximum Betweenness Centrality and  
233 the number of leafs (*Stam, 2014*). Given that Betweenness Centrality and Degree did not differ  
234 between children and adults, the observed decrease in Tree Hierarchy, in our data, is likely to be  
235 driven by a decrease in Leaf Fraction. A more straightforward quantification of network hierarchy,  
236 other than Tree Hierarchy, in complex network neuroscience is warranted though. Nevertheless,  
237 the present data point to a balance between network integration and segregation (i.e., a network  
238 topology that becomes increasingly segregated) with locally specialised regions, during childhood  
239 development.

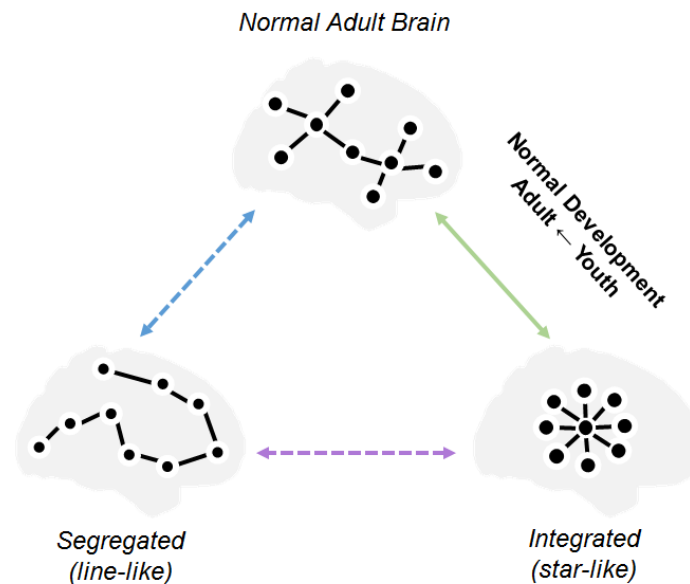
240 Most network differences in the current study are frequency-independent, suggesting that  
241 similar network constraints manifest themselves across different physiological architectures (*Barry*  
242 *et al., 2004; Bathelt et al., 2013; Murias et al., 2007*). All global MST changes in our study share  
243 the same profile across the five frequency bands between age groups. Although the specific  
244 distributed regions that showed centrality differences varied across frequency bands, there were  
245 also some frequency invariant differences: the largest number of regions that exhibited between  
246 group Eccentricity differences was found in theta and alpha mediated MSTs; regions in the fronto-  
247 parietal and default mode areas displayed the largest differences across all frequency bands. This  
248 seems to contradict some frequency-specific network findings reported in lower frequency bands  
249 in previous developmental EEG studies (*Boersma et al., 2011; Miskovic et al., 2015; Srinivasan,*  
250 *1999*). These inconsistencies may be ascribed to differences between cohorts (e.g., age-profiles) and  
251 methodological differences (e.g., the use of weighted versus unweighted graphs, use of different  
252 thresholds, and/or the normalisation of networks/graphs via random surrogates; *van Wijk et al.*  
253 *2010*). Nevertheless, MST analysis used in our study effectively addresses methodological limitations  
254 such as biased estimates of network topology and biased network comparisons (*Tewarie et al.,*  
255 *2015*).

256 Furthermore, there is now a growing understanding that conventional graph theoretical metrics  
257 (such as the clustering coefficient and shortest path length) do not fully account for fundamental  
258 properties of brain networks, and the small-world model is often used inappropriately in the field  
259 of neuroscience (*Papo et al., 2016*). Therefore, we propose here a heuristic MST model space  
260 to better capture the trajectory of changes in functional brain networks underlying normative  
261 brain development (*Figure 5*). Within this MST model space, current findings suggest a clear  
262 developmental trajectory of brain networks along the right axis, suggesting a balance between  
263 integration and segregation in topology. An adequate delineation of different trajectories of



264 topological changes in abnormal development, which may be a more useful biomarker than the  
265 absolute values (*Wolff and Piven, 2014*), can also be provided by this network space. For instance,  
266 MST networks were found to be more star-like in ADHD children compared to age-matched typical  
267 children (*Janssen et al., 2017*) - a pattern that fits with a shift towards the lower-right corner of the  
268 network space. Such a trend indicates a delay in brain maturation for ADHD children. In contrast,  
269 MST networks become more line-like in children with dyslexia compared to typically developing  
270 children (*Fraga Gonzalez et al., 2016*) - a transition to the lower-left corner of the network space.  
271 This pattern indicates an alternative developmental trajectory along the horizontal axis for brain  
272 networks in dyslexia, veering from the typical developmental trajectory along the right axis. Our  
273 model space suggests that the normal adult brain that emerges during development is a special  
274 composite that combines optimal network integration and segregation, degree diversity, and  
275 hierarchy. Moreover, distinct pathological trajectories in adults, if projecting the normal adult brain  
276 onto the horizontal axis, could also be represented in this model space: a more de-centralised  
277 line-like MST was found in patients with early relapsing remitting multiple sclerosis (*Tewarie et al.,*  
278 *2014*) and Alzheimer's disease (*Yu et al., 2016*), suggesting that networks in these diseases move  
279 towards the lower-left corner (more segregated); a more centralised star-like MST was observed in  
280 fronto-temporal dementia (*Yu et al., 2016*), indicating an opposite trend towards the lower-right  
281 corner (more integrated).

282  
283  
284  
285  
286  
287  
288  
289  
290  
291  
292  
293  
294  
295  
296  
297  
298  
299  
300



301 **Figure 5.** A heuristic minimum spanning tree (MST) model for the emergence  
302 of complex brain networks. This MST model space is based on the heuristic  
303 model of complex brain networks proposed by Stam and Van Straaten 2012.  
304 The model space consists of two extreme MSTs (representing network  
305 integration/segregation), an optimal MST for the normal adult brain, and three  
306 inter-connecting axes. Functional brain networks are proposed to develop  
307 from a star-like MST toward the optimal MST along the up-right axis, i.e., a  
308 balance between network integration and segregation. The solid line  
309 represents a developmental trajectory supported by this study, dashed lines  
310 represent trajectories that require future rigorous empirical support.

311  
312  
313  
314

There are a few caveats worth mentioning in relation to the future application of this work. From a theoretical point of view, it is conceded that there are currently no simple mathematical models that fully characterise healthy brain networks, such as its hierarchical modularity, in order to fill the gap between the existing small-world and scale-free network models. Tree Hierarchy is a composite measure of network hierarchy, and thus is inherently correlated with other measures such as leaf number and maximum betweenness centrality (see methods for details). Therefore, discovery of new mathematical models will likely support a deeper understanding of network constraints on the develop-

ing brain (*Stam and van Straaten, 2012*). From a methodological point of view, although in the present study we took care of signal leakage in source space using the leakage-invariant PLI metric, and loops were discarded in the MST construction, the data may still have suffered to some extent

315 from so-called secondary leakage (*Palva and Palva, 2012; Wang et al., 2018*). Therefore, future  
316 studies would also benefit from advanced methods such as implementing Lowdin Orthogonalisation  
317 (*Lowdin, 1950*) in MEG connectivity/network analyses to reduce those “ghost” connections  
318 (*Colclough et al., 2015*). Furthermore, for the warping procedure in children, we initially tested with  
319 age-specific paediatric templates as it was suspected that, in comparison to the adult template, the  
320 paediatric ones would produce a better approximation to the child’s brain anatomy due to better  
321 alignment in terms of skull thickness and brain morphology. However, adult and child templates  
322 produced very similar results in a previous study (*Cheyne et al., 2014*). Moreover, the AAL atlas was  
323 not available for these paediatric templates, hence using the anatomical labelling from the AAL  
324 (adult) atlas (*Tzourio-Mazoyer et al., 2002*) in paediatric surrogate structural MRI would still only  
325 provide an approximate labelling. Therefore, the surrogate procedure (using the adult template),  
326 as well as the subsequent analyses, were kept the same for all participants. Nevertheless, the  
327 use of age-specific template brain images and atlases together with surface-based registration  
328 in further studies would help to minimise registration errors due to the heterogeneity of brain  
329 anatomy in young children (*Fonov et al., 2011*). In addition, canonically-defined frequency bands  
330 may overlook some physiological mechanisms underlying the development of oscillatory neural  
331 networks. Estimating network properties from age-appropriate frequency bands is critical in future  
332 work (*Boersma et al., 2013*), for example by parameterization of neuronal power spectral densities  
333 on the basis of putative oscillatory components (*Haller et al., 2018*). Lastly, the developmental  
334 trajectory found in this cross-sectional study should be replicated in a large longitudinal sample.

335 In conclusion, a combination of an atlas-based beamformer in age-appropriate MEG data,  
336 leakage-insensitive PLI connectivity estimation, and unbiased MST network measures revealed that  
337 functional brain networks become more segregated during childhood. Increases in MST Diameter  
338 and decreases in Leaf Fraction indicate that functional networks develop into a more line-like (de-  
339 centralised) topology; increases in Degree Correlation and Eccentricity suggest that brain regions  
340 stay less central and become more locally specialised; decreases in Kappa and Tree Hierarchy  
341 emphasise that the network segregation during development balances the benefits of integration  
342 between distant brain regions against the risks of overload on central regions. Importantly, these  
343 topological network changes are most evident in the preschool years of childhood (i.e., the younger  
344 age group between 4-6 years in our data) and exhibit the same pattern for all frequency bands  
345 (i.e., delta to low gamma). Our data resolves a long-standing debate in the field with respect  
346 to the normative brain development across spatial and temporal scales of investigation using  
347 MRI-based and electrophysiological measures. Finally, we propose a heuristic MST model for the  
348 emergence of complex brain networks, in which different patterns of network abnormality could be  
349 discerned depending upon their trajectories through this “network space”. Therefore, our study also  
350 represents the first attempt in providing a unifying network model for the development of functional  
351 brain networks in youth. We anticipate new data from both normative and abnormal developmental  
352 studies to be incorporated into this network space to enable us not only to understand new  
353 mechanisms for early brain development and resolve ambiguities in the field, but most importantly  
354 to translate brain network studies into solutions for clinical diagnosis and treatments.

## 355 **Methods and Materials**

### 356 **Participants**

357 Included participants were control participants who took part in a larger project on stuttering. The  
358 dataset consisted of MEG recordings collected from 28 children and 24 adults during 3-5 minutes  
359 of eyes-open resting-state. Due to excessive head movement, incidental system noise or signs of  
360 drowsiness, data from 4 children were excluded. The present analyses were therefore completed  
361 on a total of 48 participants: 24 children aged from 4 to 12 years, and 24 adults ( $\mu = 40.6$ ,  $\sigma = 17.4$ ,  
362 16 males). Children were further divided into two groups: a younger group with mean age centred  
363 at 5 years (5 Y.O.,  $N = 10$ ,  $\mu = 5.4$ ,  $\sigma = 1.1$ , 5 males) and an older group at 10 years (10 Y.O.,  $N = 14$ ,  $\mu$

364 = 9.8,  $\sigma = 1.5$ , 12 males).

365 The experimental procedures were approved by the Human Participants Ethics Committee at  
366 Macquarie University. Written consent was obtained from the adult participants and from the  
367 parents/guardians of the children prior to the experiment. All participants were remunerated for  
368 their participation.

### 369 **Experimental Procedures**

370 Upon arriving at the laboratory, participants were familiarised with the magnetically shielded room  
371 where they would be tested in a supine position. Prior to MEG measurements, five head position  
372 indicators (HPIs) were attached to a tightly fitting elastic cap. The 3D locations of the HPIs, fiducial  
373 landmarks (nasion, and left and right pre-auricular points) and the shape of each participant's head  
374 were measured with a pen digitiser (Polhemus Fastrak, Colchester, VT, USA).

375 Children in the 5 Y.O. group were tested using the child-customized 125-channel whole-head  
376 gradiometer MEG system (Model PQ1064R-N2m, KIT, Kanazawa, Japan), and all other participants  
377 were tested using the 160-channel whole-head gradiometer MEG system (Model PQ1160RN2,  
378 KIT, Kanazawa, Japan). The gradiometers of both systems have a 50 mm baseline and 15.5 mm  
379 diameter coils, and are positioned in a glass fibre reinforced plastic cryostat for measurement of  
380 the normal component of the magnetic field from the human brain (*Kado et al., 1999*). In both  
381 systems, neighbouring channels are 38 mm apart and 20 mm from the outer dewar surface. The  
382 125-channel dewar was designed to fit a maximum head circumference of 53.4 cm, accommodating  
383 more than 90% of heads of 5-year olds (*Johnson et al., 2010*). Both systems were situated within  
384 the same magnetically shielded room, and therefore have comparable environmental noise level.

385 During MEG data acquisition, participants were asked to remain relaxed, awake and with their  
386 eyes fixed on a white cross at the centre of a black 36 cm (width) x 24 cm (length) rectangular  
387 image with 4 x 4 degrees of visual angle. The visual presentation was done by video projectors  
388 situated outside the magnetically shielded room (child MEG projector: Sharp Notevision Model  
389 PG10S, Osaka, Japan; Adult MEG projector: InFocus Model IN5108, Portland, USA). Drowsiness was  
390 monitored online through a video-camera so that any affected data would be removed from further  
391 analysis. For child participants, an experienced researcher sat with them during the whole session  
392 to make sure they were comfortable.

### 393 **MEG Data Pre-processing**

394 MEG data were acquired at a sampling frequency of 1000 Hz and with an online bandpass of  
395 0.03-200 Hz. Head positions were measured at the beginning and end of the acquisition session; a  
396 movement tolerance of 5 mm and 10 mm was used in adults and children, respectively.

397 The Yokogawa/KIT MEG data were firstly converted to a CTF data format using BrainWave toolbox  
398 developed at the Hospital for Sick Children in Canada (<http://cheynelab.utoronto.ca>, version 3.3beta,  
399 see Cheyne et al., 2014 for details). Then, the CTF compatible MEG data were imported into and  
400 processed using DataEditor in the CTF MEG5 software (VSM MedTech Systems Inc., Coquitlam BC,  
401 Canada; Version 5.0.2). The continuous raw MEG data were firstly filtered from 0.5 to 100 Hz using  
402 bi-directional IIR Butterworth filters with DC removal and segmented into epochs of 4096 samples (=  
403 4.096 seconds). Epochs that contained physiological (e.g., muscle noise) or environmental artefacts  
404 were rejected by visual inspection. The cleaned datasets consisted on average of 23.8 ( $\sigma = 3.02$ )  
405 epochs for the children and 40 epochs ( $\sigma = 0.02$ ) for the adults.

### 406 **Head Modelling and Surrogate MRIs**

407 For the head model construction, obtaining individual structural MRI scans of children - especially  
408 of those aged below 6 years - was impractical. A "surrogate" MRI approach was therefore used  
409 here to warp the adult Montreal Neurological Institute (MNI) template T1 structural brain image  
410 to each participant's digitized head shape with an iterative closest point algorithm implemented  
411 in BrainWave (see *Cheyne et al. 2014* for details). MEG data was co-registered with the warped

412 “surrogate” MRI using the digitised fiducial points. The outline of the scalp from this co-registered  
413 “surrogate” MRI was extracted using the MRIVIEWER in the CTF MEG5 software (VSM MedTech  
414 Systems Inc., Coquitlam BC, Canada; Version 5.0.2) and then used to fit a multisphere volume  
415 conductor model (*Huang et al., 1999*), which was subsequently used for the beamformer analysis  
416 described below.

### 417 **Beamforming**

418 An atlas-based beamforming approach (*Hillebrand et al., 2012*) was adopted to project sensor level  
419 MEG data to source space. The co-registered surrogate MRIs were normalised to the standard MNI  
420 (T1) template, using the SEG toolbox (*Weiskopf et al., 2011*) in SPM8. The automated anatomical  
421 labelling (AAL) atlas (*Tzourio-Mazoyer et al., 2002*) was used to label the voxels in a participant’s  
422 normalised co-registered surrogate MRI, following which the centroid for each AAL regions of  
423 interest (80 ROIs; 78 cortical and bilateral hippocampal) was inversely transformed to native space  
424 (*Hillebrand et al., 2016*).

425 For each centroid, beamformer weights were computed using Synthetic Aperture Magnetom-  
426 etry (SAM, *Robinson 1999*). This beamformer selectively weights the contribution from each MEG  
427 sensor to a voxel’s activity based on the broad-band (0.5-48 Hz) data covariance matrix, which was  
428 computed from (1) all selected time-series, (2) the forward solution (lead field) for a dipolar source  
429 with optimum orientation at that location, and (3) a unity noise covariance that was scaled by the  
430 smallest singular value in a decomposition of the data covariance matrix. The broad-band MEG data  
431 were subsequently projected through the normalised beamformer weights (*Cheyne et al. (2007)*).

432 From the resulting time-series, the first 15 artifact-free epochs, containing 4096 samples (= 4.096  
433 seconds), were selected for further analyses of functional connectivity and network topology. These  
434 selected epochs were then band-pass filtered, using an offline discrete Fast Fourier Transform filter  
435 without phase distortion, as implemented in the BrainWave toolbox developed at VU University  
436 Medical Centre (C.J. Stam; <http://home.kpn.nl/stam7883/brainwave.html>, version 0.9.152.4.1), into  
437 five canonical MEG frequency bands (delta: 0.5–4 Hz, theta: 4–8 Hz, alpha: 8–13 Hz, beta: 13–30  
438 Hz, and low gamma: 30–48 Hz). Subsequently, the instantaneous phase for each time-series was  
439 determined by taking the argument of the analytic signal as computed using the Hilbert transform  
440 (*Marple, 1999*).

### 441 **Connectivity Analysis**

442 Pair-wise frequency band-specific functional connectivity between the 80 ROIs was estimated using  
443 the phase lag index (PLI) for each of the 15 artifact-free epochs (= 4.096 seconds). PLI reflects the  
444 consistency by which one signal is phase leading or lagging with respect to another signal (*Stam*  
445 *et al., 2007*), which can be expressed as:

$$446 \quad PLI = |\langle \text{sign}[\sin \Delta\varphi(t_k)] \rangle| \quad (1)$$

447 where  $\Delta\varphi$  refers to the instantaneous phase difference between two time-series,  $t_k$  are discrete  
448 time steps calculated over all  $K = 1 \dots N$ ,  $\text{sign}$  refers to the signum function,  $\langle \rangle$  and  $||$  denote  
449 the mean and absolute value, respectively. Specifically, PLI quantifies phase synchronisation as a  
450 measure of the asymmetry in the distribution of instantaneous phase differences between two  
451 time-series (in our case the beamformer reconstructed time-series for two ROIs). The value of PLI  
452 ranges from zero (random phase differences/no functional connectivity or only zero-lag/mod  $\pi$ ) and  
453 one (perfect non-zero-lag synchrony). Because the effects of volume conduction/field spread/signal  
454 leakage give zero-lag (mod  $\pi$ ) phase differences, PLI is insensitive to these effects at the cost of  
455 being blind to true zero-lag interactions. For each frequency band and each epoch, the 80 x 80  
456 connectivity matrix of pairwise PLI values was computed. ROI-PLI was computed as the average PLI  
457 between a node and all other nodes, and whole-brain PLI was calculated as the average across all  
458 nodal PLI values.



## 458 **Minimum Spanning Tree Analysis**

459 For each epoch and participant separately, the minimum spanning tree (MST) sub-graph was  
460 constructed using the PLI connectivity matrix. The MST is constructed by connecting all  $n$  nodes in  
461 such a way that the cost (the sum of all link weights) is minimised without forming cycles. For the  
462 computation of the MST,  $1/PLI$  is used as the link weights since we are interested in the strongest  
463 connections in the network. MSTs were constructed in BrainWave by applying Kruskal's algorithm  
464 (*Kruskal, 1956*), which starts with an unconnected network, adds the link with lowest weight, then  
465 adds the link with next lowest weight (if this does not create a loop), until all nodes are connected,  
466 thereby forming a tree consisting of  $m = n - 1$  links.

467 Two extreme tree topologies exist: (1) a line-like tree (A in *Figure 1*) where all nodes are connected  
468 to two other nodes with the exception of the two so-called "leaf-nodes" at either end that have  
469 only one link, and (2) a star-like tree (C in *Figure 1*) where all leaves are connected to one central  
470 node. There are many different tree types between these two extremes (e.g., B in *Figure 1*). The  
471 tree topology can be characterised with various measures (*Boersma et al., 2013*).

472 Global MST network measures are informative about the functional integration and segregation  
473 of the entire network. Five different global MST measures were used here: (1) the "Leaf Fraction" is  
474 computed as the number of leaf nodes, divided by the total number of nodes; (2) the "Diameter"  
475 is the longest shortest path between any two nodes, where the shortest path is defined as the  
476 path with smallest number of links between two nodes; (3) the "Tree Hierarchy" was introduced  
477 (*Boersma et al., 2013*) to describe a balance between a small diameter without overloading central  
478 nodes in the tree (*Figure 1*). It is defined as  $T_H = \frac{l}{2mBC_{max}}$ , where  $l$  is the leaf number and  $BC_{max}$   
479 represents the maximal betweenness centrality in the tree. In a line-like tree,  $l = 2$  and with  $m$   
480 approaching infinity,  $T_H$  approaches 0; and in a star-like tree,  $l \approx m$ , so  $T_H$  approaches 0.5; for  
481  $l$  between these two extremes,  $T_H$  can have higher values (with an upper bound of 1); (4) the  
482 "Degree Correlation" is an index of whether the degree of a node is correlated with the degree  
483 of its neighbouring nodes (*Van Mieghem et al., 2010*); (5) "Kappa" (also called degree divergence;  
484 *Barrat et al. 2008*) measures the broadness of the degree distribution, and is high in graphs with a  
485 scale-free degree distribution, and low in graphs with a degree distribution that approaches the  
486 normal distribution. Kappa also relates to network robustness: high kappa reflects high resilience  
487 against random damage in networks.

488 Nodal MST network measures capture the importance of a node within the network. Three  
489 different nodal measures for centrality ("hubness") were used: (1) the "Degree" is the number of  
490 connections of a node to its neighbouring nodes; (2) the "Betweenness Centrality" is the fraction of  
491 the shortest paths that pass through a node; (3) the "Eccentricity" of a node is the longest shortest  
492 path between a node and any other node, and is low if the node is central in the graph (*Bullmore  
493 and Sporns, 2012*).

## 494 **Statistical Analysis**

495 Statistical analyses were performed using permutation testing as implemented in the Resampling  
496 Statistical Toolkit for Matlab 2016a. We used 50,000 permutations of group membership to empiri-  
497 cally approximate the distribution for the null hypothesis (i.e., no difference between groups) for  
498 each contrast. For each permutation, the F/t values were derived for a contrast of interest, and any  
499 F/t values for the original data that exceeded the significance threshold for the F/t distribution were  
500 deemed reliable. Furthermore,  $p$  values were corrected for multiple comparisons at the threshold  
501 of 0.05 using the false discovery rate (FDR, *Benjamini and Hochberg 1995*).

502 For each frequency band and each participant separately, whole-brain PLI were averaged over  
503 the 15 epochs per participant. The ROI-PLI values, global and nodal MST measures were averaged  
504 over 15 epochs, yielding 80 ROI-PLI, 5 global MST, and  $3 \times 80$  (= nodal MST measures  $\times$  ROIs) values  
505 per participant for each frequency band, respectively.

506 Permutation tests were initially performed, for each frequency band separately, between adults  
507 and children (as a whole group), for the whole-brain PLI and the global MST measures (FDR corrected

508 for the number of global measures (5)); if the whole-brain PLI or the global MST measures were  
509 significantly different in a specific frequency band, then the ROI-PLI and the nodal MST measures  
510 were compared (FDR corrected for three nodal measures x 80 ROIs). Second level permutation tests  
511 were performed in pairwise groups (10 Y.O. versus 5 Y.O., adults versus 5 Y.O., adults versus 10 Y.O.)  
512 for the whole-brain PLI or the global MST measures if adults and children (as a whole group) showed  
513 significant differences for these measures in any specific frequency band, and for the ROI-PLI or the  
514 nodal MST measures if these measures were significantly different in any specific frequency band  
515 between adults and children (as a whole group).

## 516 Acknowledgments

517 We thank all participants for their participation. We also thank Douglas Cheyne and Cecilia Jobst  
518 for their assistance in the preliminary data analysis. Finally, we acknowledge the collaboration of  
519 Kanazawa Institute of Technology in establishing the KIT-Macquarie MEG laboratory.

## 520 Additional information

### 521 Funding

522 This work was supported by the Australian Research Council (ARC) Centre of Excellence for Cognition  
523 and its Disorders (grant number CE110001021, <http://www.ccd.edu.au>), and the ARC Discovery  
524 Project (DP170103148). Wei He was supported by the Macquarie University Research Fellowship  
525 (MQRF) (IRIS Project: 9201501199). Paul F. Sowman was supported by the National Health and  
526 Medical Research Council, Australia (#1003760) and the Australian Research Council (DE130100868).

### 527 Author contributions

528 Wei He: conceptualisation, funding acquisition, data curation, formal analysis, validation, visualisa-  
529 tion, methodology, writing (original draft, reviewing and editing); Paul F Sowman: conceptualisation,  
530 funding acquisition, data collection, writing (reviewing and editing); Jon Brock: conceptualisation,  
531 funding acquisition, writing (reviewing and editing); Andrew C. Etchell: project management, data  
532 collection and curation; Cornelis J. Stam: conceptualisation, resources, methodology, writing (re-  
533 viewing and editing); Arjan Hillebrand: conceptualisation, resources, formal analysis, validation,  
534 visualisation, methodology, supervision, writing (original draft, reviewing and editing).

## 535 References

- 536 **Antiqueira L**, Rodrigues FA, van Wijk BC, Costa Lda F, Daffertshofer A. Estimating complex cortical networks via  
537 surface recordings- a critical note. *Neuroimage*. 2010; 53(2):439–49. doi: [10.1016/j.neuroimage.2010.06.018](https://doi.org/10.1016/j.neuroimage.2010.06.018).
- 538 **Barabasi AL**, Albert R. Emergence of scaling in random networks. *Science*. 1999; 286(5439):509–12.
- 539 **Barrat A**, Barthélemy M, Vespignani A. *Dynamical Processes on Complex Networks*. Cambridge: Cambridge  
540 University Press; 2008. doi: DOI: [10.1017/CBO9780511791383](https://doi.org/10.1017/CBO9780511791383).
- 541 **Barratt EL**, Francis ST, Morris PG, Brookes MJ. Mapping the topological organisation of beta oscillations in  
542 motor cortex using MEG. *Neuroimage*. 2018; doi: [10.1016/j.neuroimage.2018.06.041](https://doi.org/10.1016/j.neuroimage.2018.06.041).
- 543 **Barry RJ**, Clarke AR, McCarthy R, Selikowitz M, Johnstone SJ, Rushby JA. Age and gender effects in EEG  
544 coherence: I. Developmental trends in normal children. *Clin Neurophysiol*. 2004; 115(10):2252–8. doi:  
545 [10.1016/j.clinph.2004.05.004](https://doi.org/10.1016/j.clinph.2004.05.004).
- 546 **Bathelt J**, O'Reilly H, Clayden JD, Cross JH, de Haan M. Functional brain network organisation of children  
547 between 2 and 5 years derived from reconstructed activity of cortical sources of high-density EEG recordings.  
548 *Neuroimage*. 2013; 82:595–604. doi: [10.1016/j.neuroimage.2013.06.003](https://doi.org/10.1016/j.neuroimage.2013.06.003).
- 549 **Baum GL**, Ciric R, Roalf DR, Betzel RF, Moore TM, Shinohara RT, Kahn AE, Vandekar SN, Rupert PE, Quarmley M,  
550 Cook PA, Elliott MA, Ruparel K, Gur RE, Gur RC, Bassett DS, Satterthwaite TD. Modular Segregation of Structural  
551 Brain Networks Supports the Development of Executive Function in Youth. *Curr Biol*. 2017; 27(11):1561–1572  
552 e8. doi: [10.1016/j.cub.2017.04.051](https://doi.org/10.1016/j.cub.2017.04.051).
- 553 **Benjamini Y**, Hochberg Y. Controlling the false discovery rate: a practical and powerful approach to multiple  
554 testing. *Journal of the royal statistical society*. 1995; Series B (Methodological):289–300.

- 555 **de Bie HM**, Boersma M, Adriaanse S, Veltman DJ, Wink AM, Roosendaal SD, Barkhof F, Stam CJ, Oostrom KJ,  
556 Delemarre-van de Waal HA, Sanz-Arigita EJ. Resting-state networks in awake five- to eight-year old children.  
557 *Hum Brain Mapp.* 2012; 33(5):1189–201. doi: [10.1002/hbm.21280](https://doi.org/10.1002/hbm.21280).
- 558 **Boersma M**, Smit DJ, de Bie HM, Van Baal GC, Boomsma DI, de Geus EJ, Delemarre-van de Waal HA, Stam CJ.  
559 Network analysis of resting state EEG in the developing young brain: structure comes with maturation. *Hum*  
560 *Brain Mapp.* 2011; 32(3):413–25. doi: [10.1002/hbm.21030](https://doi.org/10.1002/hbm.21030).
- 561 **Boersma M**, Smit DJ, Boomsma DI, De Geus EJ, Delemarre-van de Waal HA, Stam CJ. Growing trees in child  
562 brains: graph theoretical analysis of electroencephalography-derived minimum spanning tree in 5- and  
563 7-year-old children reflects brain maturation. *Brain Connect.* 2013; 3(1):50–60. doi: [10.1089/brain.2012.0106](https://doi.org/10.1089/brain.2012.0106).
- 564 **Brookes MJ**, Woolrich M, Luckhoo H, Price D, Hale JR, Stephenson MC, Barnes GR, Smith SM, Morris PG.  
565 Investigating the electrophysiological basis of resting state networks using magnetoencephalography. *Proc*  
566 *Natl Acad Sci U S A.* 2011; 108(40):16783–8. doi: [10.1073/pnas.1112685108](https://doi.org/10.1073/pnas.1112685108).
- 567 **Bullmore E**, Barnes A, Bassett DS, Fornito A, Kitzbichler M, Meunier D, Suckling J. Generic aspects of  
568 complexity in brain imaging data and other biological systems. *Neuroimage.* 2009; 47(3):1125–34. doi:  
569 [10.1016/j.neuroimage.2009.05.032](https://doi.org/10.1016/j.neuroimage.2009.05.032).
- 570 **Bullmore E**, Sporns O. The economy of brain network organization. *Nat Rev Neurosci.* 2012; 13(5):336–49. doi:  
571 [10.1038/nrn3214](https://doi.org/10.1038/nrn3214).
- 572 **Cheyne D**, Bostan AC, Gaetz W, Pang EW. Event-related beamforming: a robust method for presurgical functional  
573 mapping using MEG. *Clin Neurophysiol.* 2007; 118(8):1691–704. doi: [10.1016/j.clinph.2007.05.064](https://doi.org/10.1016/j.clinph.2007.05.064).
- 574 **Cheyne D**, Jobst C, Tesan G, Crain S, Johnson B. Movement-related neuromagnetic fields in preschool age  
575 children. *Hum Brain Mapp.* 2014; 35(9):4858–75. doi: [10.1002/hbm.22518](https://doi.org/10.1002/hbm.22518).
- 576 **Colclough GL**, Brookes MJ, Smith SM, Woolrich MW. A symmetric multivariate leakage correction for MEG  
577 connectomes. *Neuroimage.* 2015; 117:439–48. doi: [10.1016/j.neuroimage.2015.03.071](https://doi.org/10.1016/j.neuroimage.2015.03.071).
- 578 **Crossley NA**, Mechelli A, Scott J, Carletti F, Fox PT, McGuire P, Bullmore ET. The hubs of the human connec-  
579 tome are generally implicated in the anatomy of brain disorders. *Brain.* 2014; 137(Pt 8):2382–95. doi:  
580 [10.1093/brain/awu132](https://doi.org/10.1093/brain/awu132).
- 581 **van Dellen E**, Sommer IE, Bohlken MM, Tewarie P, Draaisma L, Zalesky A, Di Biase M, Brown JA, Douw L, Otte  
582 WM, Mandl RCW, Stam CJ. Minimum spanning tree analysis of the human connectome. *Hum Brain Mapp.*  
583 2018; doi: [10.1002/hbm.24014](https://doi.org/10.1002/hbm.24014).
- 584 **DeSalvo MN**, Douw L, Tanaka N, Reinsberger C, Stufflebeam SM. Altered structural connectome in temporal  
585 lobe epilepsy. *Radiology.* 2014; 270(3):842–8. doi: [10.1148/radiol.13131044](https://doi.org/10.1148/radiol.13131044).
- 586 **Dominguez LG**, Wennberg R, Velazquez JLP, Erra RG. Enhanced measured synchronization of unsynchronized  
587 sources: inspecting the physiological significance of synchronization analysis of whole brain electrophysiological  
588 recordings. *International Journal of Physical Sciences.* 2007; 2(11):305–317.
- 589 **Erdős P**, Rényi A. On random graphs. *Publications Mathematicae (Debrecen).* 1959; 6:290–297.
- 590 **Fair DA**, Cohen AL, Power JD, Dosenbach NU, Church JA, Miezin FM, Schlaggar BL, Petersen SE. Functional brain  
591 networks develop from a "local to distributed" organization. *PLoS Comput Biol.* 2009; 5(5):e1000381. doi:  
592 [10.1371/journal.pcbi.1000381](https://doi.org/10.1371/journal.pcbi.1000381).
- 593 **Fonov V**, Evans AC, Botteron K, Almli CR, McKinstry RC, Collins DL, Brain Development Cooperative G. Un-  
594 biased average age-appropriate atlases for pediatric studies. *Neuroimage.* 2011; 54(1):313–27. doi:  
595 [10.1016/j.neuroimage.2010.07.033](https://doi.org/10.1016/j.neuroimage.2010.07.033).
- 596 **Fornito A**, Zalesky A, Bassett DS, Meunier D, Ellison-Wright I, Yucel M, Wood SJ, Shaw K, O'Connor J, Nertney  
597 D, Mowry BJ, Pantelis C, Bullmore ET. Genetic influences on cost-efficient organization of human cortical  
598 functional networks. *J Neurosci.* 2011; 31(9):3261–70. doi: [10.1523/JNEUROSCI.4858-10.2011](https://doi.org/10.1523/JNEUROSCI.4858-10.2011).
- 599 **Fraga Gonzalez G**, Van der Molen MJW, Zaric G, Bonte M, Tijms J, Blomert L, Stam CJ, Van der Molen MW. Graph  
600 analysis of EEG resting state functional networks in dyslexic readers. *Clin Neurophysiol.* 2016; 127(9):3165–  
601 3175. doi: [10.1016/j.clinph.2016.06.023](https://doi.org/10.1016/j.clinph.2016.06.023).
- 602 **Grayson DS**, Fair DA. Development of large-scale functional networks from birth to adulthood: A guide to the  
603 neuroimaging literature. *Neuroimage.* 2017; doi: [10.1016/j.neuroimage.2017.01.079](https://doi.org/10.1016/j.neuroimage.2017.01.079).

- 604 **Gu S**, Satterthwaite TD, Medaglia JD, Yang M, Gur RE, Gur RC, Bassett DS. Emergence of system roles in normative  
605 neurodevelopment. *Proc Natl Acad Sci U S A*. 2015; 112(44):13681–6. doi: [10.1073/pnas.1502829112](https://doi.org/10.1073/pnas.1502829112).
- 606 **Haller M**, Donoghue T, Peterson E, Varma P, Sebastian P, Gao R, Noto T, Knight RT, Shestyuk A, Voytek B.  
607 Parameterizing neural power spectra. *bioRxiv*. 2018; p. 299859.
- 608 **He W**, Brock J, Johnson BW. Face-sensitive brain responses measured from a four-year-old child with  
609 a custom-sized child MEG system. *Journal of Neuroscience Methods*. 2014; 222(0):213–217. doi:  
610 <http://dx.doi.org/10.1016/j.jneumeth.2013.11.020>.
- 611 **Hillebrand A**, Barnes GR, Bosboom JL, Berendse HW, Stam CJ. Frequency-dependent functional connectivity  
612 within resting-state networks: an atlas-based MEG beamformer solution. *Neuroimage*. 2012; 59(4):3909–21.  
613 doi: [10.1016/j.neuroimage.2011.11.005](https://doi.org/10.1016/j.neuroimage.2011.11.005).
- 614 **Hillebrand A**, Singh KD, Holliday IE, Furlong PL, Barnes GR. A new approach to neuroimaging with magnetoen-  
615 cephalography. *Hum Brain Mapp*. 2005; 25(2):199–211. doi: [10.1002/hbm.20102](https://doi.org/10.1002/hbm.20102).
- 616 **Hillebrand A**, Tewarie P, van Dellen E, Yu M, Carbo EW, Douw L, Gouw AA, van Straaten EC, Stam CJ. Direction of  
617 information flow in large-scale resting-state networks is frequency-dependent. *Proc Natl Acad Sci U S A*. 2016;  
618 113(14):3867–72. doi: [10.1073/pnas.1515657113](https://doi.org/10.1073/pnas.1515657113).
- 619 **Huang H**, Shu N, Mishra V, Jeon T, Chalak L, Wang ZJ, Rollins N, Gong G, Cheng H, Peng Y, Dong Q, He Y.  
620 Development of human brain structural networks through infancy and childhood. *Cereb Cortex*. 2015;  
621 25(5):1389–404. doi: [10.1093/cercor/bht335](https://doi.org/10.1093/cercor/bht335).
- 622 **Huang MX**, Mosher JC, Leahy RM. A sensor-weighted overlapping-sphere head model and exhaustive head  
623 model comparison for MEG. *Phys Med Biol*. 1999; 44(2):423–40.
- 624 **Janssen TWP**, Hillebrand A, Gouw A, Gelade K, Van Mourik R, Maras A, Oosterlaan J. Neural network topology  
625 in ADHD; evidence for maturational delay and default-mode network alterations. *Clin Neurophysiol*. 2017;  
626 128(11):2258–2267. doi: [10.1016/j.clinph.2017.09.004](https://doi.org/10.1016/j.clinph.2017.09.004).
- 627 **Jinhui W**, Liang W, Yufeng Z, Hong Y, Hehan T, Qiyong G, Zhang C, Chaozhe Z, Yong H. Parcellation-dependent  
628 small-world brain functional networks: A resting-state fMRI study. *Human Brain Mapping*. 2009; 30(5):1511–  
629 1523. doi: [doi:10.1002/hbm.20623](https://doi.org/10.1002/hbm.20623).
- 630 **Johnson BW**, Crain S, Thornton R, Tesan G, Reid M. Measurement of brain function in pre-school children using  
631 a custom sized whole-head MEG sensor array. *Clinical neurophysiology : official journal of the International  
632 Federation of Clinical Neurophysiology*. 2010; 121(3):340–9. doi: [10.1016/j.clinph.2009.10.017](https://doi.org/10.1016/j.clinph.2009.10.017).
- 633 **Kado H**, Higuchi M, Shimogawara M, Haruta Y, Adachi Y, Kawai J, Ogata H, Uehara G. Magnetoencephalogram  
634 systems developed at KIT. *Ieee Transactions on Applied Superconductivity*. 1999; 9(2):4057–4062. doi: [Doi  
635 10.1109/77.783918](https://doi.org/10.1109/77.783918).
- 636 **Kruskal J**. On the shortest spanning subtree of a graph and the traveling salesman problem. *Proceedings of  
637 the American Mathematical society*. 1956; 7(1):48–50.
- 638 **Lai M**, Demuru M, Hillebrand A, Fraschini M. A Comparison Between Scalp-And Source-Reconstructed EEG  
639 Networks. *bioRxiv*. 2017; p. 121764.
- 640 **Lowdin PO**. On the Non-Orthogonality Problem Connected with the Use of Atomic Wave Functions in the  
641 Theory of Molecules and Crystals. *Journal of Chemical Physics*. 1950; 18:365–375.
- 642 **Meunier D**, Achard S, Morcom A, Bullmore E. Age-related changes in modular organization of human brain  
643 functional networks. *Neuroimage*. 2009; 44(3):715–23. doi: [10.1016/j.neuroimage.2008.09.062](https://doi.org/10.1016/j.neuroimage.2008.09.062).
- 644 **Miskovic V**, Ma X, Chou CA, Fan M, Owens M, Sayama H, Gibb BE. Developmental changes in spontaneous  
645 electrocortical activity and network organization from early to late childhood. *Neuroimage*. 2015; 118:237–47.  
646 doi: [10.1016/j.neuroimage.2015.06.013](https://doi.org/10.1016/j.neuroimage.2015.06.013).
- 647 **Mulder HM**. Julius Petersen's theory of regular graphs. *Discrete Mathematics*. 1992; 100(1):157–175. doi:  
648 [https://doi.org/10.1016/0012-365X\(92\)90639-W](https://doi.org/10.1016/0012-365X(92)90639-W).
- 649 **Murias M**, Swanson JM, Srinivasan R. Functional connectivity of frontal cortex in healthy and ADHD children  
650 reflected in EEG coherence. *Cereb Cortex*. 2007; 17(8):1788–99. doi: [10.1093/cercor/bhl089](https://doi.org/10.1093/cercor/bhl089).



- 651 **Otte WM**, van Diessen E, Paul S, Ramaswamy R, Subramanyam Rallabandi VP, Stam CJ, Roy PK. Aging al-  
652 terations in whole-brain networks during adulthood mapped with the minimum spanning tree indices:  
653 the interplay of density, connectivity cost and life-time trajectory. *Neuroimage*. 2015; 109:171–89. doi:  
654 [10.1016/j.neuroimage.2015.01.011](https://doi.org/10.1016/j.neuroimage.2015.01.011).
- 655 **Palva S**, Palva JM. Discovering oscillatory interaction networks with M/EEG: challenges and breakthroughs.  
656 *Trends Cogn Sci*. 2012; 16(4):219–30. doi: [10.1016/j.tics.2012.02.004](https://doi.org/10.1016/j.tics.2012.02.004).
- 657 **Papo D**, Zanin M, Martinez JH, Buldu JM. Beware of the Small-World Neuroscientist! *Front Hum Neurosci*. 2016;  
658 10:96. doi: [10.3389/fnhum.2016.00096](https://doi.org/10.3389/fnhum.2016.00096).
- 659 **Poldrack RA**. Interpreting developmental changes in neuroimaging signals. *Hum Brain Mapp*. 2010; 31(6):872–8.  
660 doi: [10.1002/hbm.21039](https://doi.org/10.1002/hbm.21039).
- 661 **Power JD**, Cohen AL, Nelson SM, Wig GS, Barnes KA, Church JA, Vogel AC, Laumann TO, Miezin FM, Schlaggar  
662 BL, Petersen SE. Functional network organization of the human brain. *Neuron*. 2011; 72(4):665–78. doi:  
663 [10.1016/j.neuron.2011.09.006](https://doi.org/10.1016/j.neuron.2011.09.006).
- 664 **Richmond S**, Johnson KA, Seal ML, Allen NB, Whittle S. Development of brain networks and relevance of  
665 environmental and genetic factors: A systematic review. *Neurosci Biobehav Rev*. 2016; 71:215–239. doi:  
666 [10.1016/j.neubiorev.2016.08.024](https://doi.org/10.1016/j.neubiorev.2016.08.024).
- 667 **Robinson SE**. Functional neuroimaging by synthetic aperture magnetometry (SAM). Recent advances in  
668 biomagnetism. 1999; p. 302–305.
- 669 **Rubinov M**, Sporns O. Complex network measures of brain connectivity: uses and interpretations. *Neuroimage*.  
670 2010; 52(3):1059–69. doi: [10.1016/j.neuroimage.2009.10.003](https://doi.org/10.1016/j.neuroimage.2009.10.003).
- 671 **Schafer CB**, Morgan BR, Ye AX, Taylor MJ, Doesburg SM. Oscillations, networks, and their development: MEG  
672 connectivity changes with age. *Hum Brain Mapp*. 2014; 35(10):5249–61. doi: [10.1002/hbm.22547](https://doi.org/10.1002/hbm.22547).
- 673 **Schoffelen JM**, Gross J. Source connectivity analysis with MEG and EEG. *Hum Brain Mapp*. 2009; 30(6):1857–65.  
674 doi: [10.1002/hbm.20745](https://doi.org/10.1002/hbm.20745).
- 675 **Smit DJ**, de Geus EJ, Boersma M, Boomsma DI, Stam CJ. Life-Span Development of Brain Network Integration  
676 Assessed with Phase Lag Index Connectivity and Minimum Spanning Tree Graphs. *Brain Connect*. 2016;  
677 6(4):312–25. doi: [10.1089/brain.2015.0359](https://doi.org/10.1089/brain.2015.0359).
- 678 **Smith K**, Politte D, Reiker G, Nolan TS, Hildebolt C, Mattson C, Tucker D, Prior F, Turovets S, Larson-Prior LJ.  
679 Automated measurement of pediatric cranial bone thickness and density from clinical computed tomography.  
680 *Conf Proc IEEE Eng Med Biol Soc*. 2012; 2012:4462–5. doi: [10.1109/EMBC.2012.6346957](https://doi.org/10.1109/EMBC.2012.6346957).
- 681 **Sporns O**. Structure and function of complex brain networks. *Dialogues Clin Neurosci*. 2013; 15(3):247–62.
- 682 **Srinivasan R**. Spatial structure of the human alpha rhythm: global correlation in adults and local correlation in  
683 children. *Clin Neurophysiol*. 1999; 110(8):1351–62.
- 684 **Stam CJ**. Modern network science of neurological disorders. *Nat Rev Neurosci*. 2014; 15(10):683–95. doi:  
685 [10.1038/nrn3801](https://doi.org/10.1038/nrn3801).
- 686 **Stam CJ**, de Haan W, Daffertshofer A, Jones BF, Manshanden I, van Cappellen van Walsum AM, Montez T,  
687 Verbunt JP, de Munck JC, van Dijk BW, Berendse HW, Scheltens P. Graph theoretical analysis of magne-  
688 toencephalographic functional connectivity in Alzheimer's disease. *Brain*. 2009; 132(Pt 1):213–24. doi:  
689 [10.1093/brain/awn262](https://doi.org/10.1093/brain/awn262).
- 690 **Stam CJ**, Nolte G, Daffertshofer A. Phase lag index: assessment of functional connectivity from multi channel  
691 EEG and MEG with diminished bias from common sources. *Hum Brain Mapp*. 2007; 28(11):1178–93. doi:  
692 [10.1002/hbm.20346](https://doi.org/10.1002/hbm.20346).
- 693 **Stam CJ**, van Straaten ECW. The organization of physiological brain networks. *Clinical Neurophysiology*. 2012;  
694 123(6):1067–1087. doi: [10.1016/j.clinph.2012.01.011](https://doi.org/10.1016/j.clinph.2012.01.011).
- 695 **Supekar K**, Musen M, Menon V. Development of large-scale functional brain networks in children. *PLoS Biol*.  
696 2009; 7(7):e1000157. doi: [10.1371/journal.pbio.1000157](https://doi.org/10.1371/journal.pbio.1000157).
- 697 **Tewarie P**, van Dellen E, Hillebrand A, Stam CJ. The minimum spanning tree: an unbiased method for brain  
698 network analysis. *Neuroimage*. 2015; 104:177–88. doi: [10.1016/j.neuroimage.2014.10.015](https://doi.org/10.1016/j.neuroimage.2014.10.015).

- 699 **Tewarie P**, Hillebrand A, van Dijk BW, Stam CJ, O'Neill GC, Van Mieghem P, Meier JM, Woolrich MW, Morris  
700 PG, Brookes MJ. Integrating cross-frequency and within band functional networks in resting-state MEG: A  
701 multi-layer network approach. *Neuroimage*. 2016; 142:324–336. doi: [10.1016/j.neuroimage.2016.07.057](https://doi.org/10.1016/j.neuroimage.2016.07.057).
- 702 **Tewarie P**, Hillebrand A, Schoonheim MM, van Dijk BW, Geurts JJG, Barkhof F, Polman CH, Stam CJ. Functional  
703 brain network analysis using minimum spanning trees in Multiple Sclerosis: An MEG source-space study.  
704 *NeuroImage*. 2014; 88:308–318. doi: <https://doi.org/10.1016/j.neuroimage.2013.10.022>.
- 705 **Toth B**, Urban G, Haden GP, Mark M, Torok M, Stam CJ, Winkler I. Large-scale network organization of EEG  
706 functional connectivity in newborn infants. *Hum Brain Mapp*. 2017; 38(8):4019–4033. doi: [10.1002/hbm.23645](https://doi.org/10.1002/hbm.23645).
- 707 **Troeblinger L**, Lopez JD, Lutti A, Bestmann S, Barnes G. Discrimination of cortical laminae using MEG. *Neuroim-*  
708 *age*. 2014; 102 Pt 2:885–93. doi: [10.1016/j.neuroimage.2014.07.015](https://doi.org/10.1016/j.neuroimage.2014.07.015).
- 709 **Tzourio-Mazoyer N**, Landeau B, Papathanassiou D, Crivello F, Etard O, Delcroix N, Mazoyer B, Joliot M. Auto-  
710 mated anatomical labeling of activations in SPM using a macroscopic anatomical parcellation of the MNI MRI  
711 single-subject brain. *Neuroimage*. 2002; 15(1):273–89. doi: [10.1006/nimg.2001.0978](https://doi.org/10.1006/nimg.2001.0978).
- 712 **Van Mieghem P**, Wang H, Ge X, Tang S, Kuipers FA. Influence of assortativity and degree-preserving rewiring on  
713 the spectra of networks. *European Physical Journal B*. 2010; 76(4):643–652. doi: [10.1140/epjb/e2010-00219-x](https://doi.org/10.1140/epjb/e2010-00219-x).
- 714 **Wang H**, Hernandez JM, Van Mieghem P. Betweenness centrality in a weighted network. *Phys Rev E Stat Nonlin*  
715 *Soft Matter Phys*. 2008; 77(4 Pt 2):046105. doi: [10.1103/PhysRevE.77.046105](https://doi.org/10.1103/PhysRevE.77.046105).
- 716 **Wang SH**, Lobier M, Siebenhuhner F, Puolivali T, Palva S, Palva JM. Hyperedge bundling: A practical solution  
717 to spurious interactions in MEG/EEG source connectivity analyses. *Neuroimage*. 2018; 173:610–622. doi:  
718 [10.1016/j.neuroimage.2018.01.056](https://doi.org/10.1016/j.neuroimage.2018.01.056).
- 719 **Weiskopf N**, Lutti A, Helms G, Novak M, Ashburner J, Hutton C. Unified segmentation based correction of  
720 R1 brain maps for RF transmit field inhomogeneities (UNICORT). *Neuroimage*. 2011; 54(3):2116–24. doi:  
721 [10.1016/j.neuroimage.2010.10.023](https://doi.org/10.1016/j.neuroimage.2010.10.023).
- 722 **Wig GS**. Segregated Systems of Human Brain Networks. *Trends Cogn Sci*. 2017; 21(12):981–996. doi:  
723 [10.1016/j.tics.2017.09.006](https://doi.org/10.1016/j.tics.2017.09.006).
- 724 **van Wijk BC**, Stam CJ, Daffertshofer A. Comparing brain networks of different size and connectivity density  
725 using graph theory. *PLoS One*. 2010; 5(10):e13701. doi: [10.1371/journal.pone.0013701](https://doi.org/10.1371/journal.pone.0013701).
- 726 **Wolff JJ**, Piven J. Neurodevelopmental disorders: Accelerating progress in autism through developmental  
727 research. *Nat Rev Neurol*. 2014; 10(8):431–2. doi: [10.1038/nrneurol.2014.126](https://doi.org/10.1038/nrneurol.2014.126).
- 728 **Yu M**, Engels MMA, Hillebrand A, van Straaten ECW, Gouw AA, Teunissen C, van der Flier WM, Scheltens P, Stam  
729 CJ. Selective impairment of hippocampus and posterior hub areas in Alzheimer's disease: an MEG-based  
730 multiplex network study. *Brain*. 2017; 140(5):1466–1485. doi: [10.1093/brain/awx050](https://doi.org/10.1093/brain/awx050).
- 731 **Yu M**, Gouw AA, Hillebrand A, Tijms BM, Stam CJ, van Straaten EC, Pijnenburg YA. Different functional connectivity  
732 and network topology in behavioral variant of frontotemporal dementia and Alzheimer's disease: an EEG  
733 study. *Neurobiol Aging*. 2016; 42:150–62. doi: [10.1016/j.neurobiolaging.2016.03.018](https://doi.org/10.1016/j.neurobiolaging.2016.03.018).

734 **Appendix 1**

735 **Appendix 1 Table 1.** Regions of interest (ROIs) that manifest significant Eccentricity differences  
 736 between groups in the delta band.

ROIs	Pairwise Permutation Comparisons (FDR-corrected)			
	Children (N = 24) vs Adults (N = 24)	5 Y.O. (N = 10) vs 10 Y.O. (N = 14)	5 Y.O. (N = 10) vs Adults (N = 24)	10 Y.O. (N=14) vs Adults (N=24)
<b>Left Hemisphere</b>				
Gryus Rectus			↑	
Olfactory Cortex			↑	
Superior frontal gyrus, orbital part	↑		↑	
Frontal gyrus, medial orbital part				
Middle frontal gyrus, orbital part	↑		↑	
Inferior frontal gyrus, orbital part	↑		↑	
Superior frontal gyrus			↑	
Middle frontal gyrus			↑	
Inferior frontal gyrus, opercular part			↑	
Inferior frontal gyrus, triangular part	↑		↑	
Superior frontal gyrus, medial			↑	
Supplementary motor area			↑	
Paracentral lobule				
Precentral gyrus		↑	↑	
Rolandic operculum			↑	
Postcentral gyrus				
Superior parietal gyrus		↑	↑	
Inferior parietal, but supramarginal and angular gyri			↑	
Supramarginal gyrus				
Angular gyrus			↑	
Precuneus	↑		↑	
Superior occipital gyrus		↑		
Middle occipital gyrus			↑	
Inferior occipital gyrus		↑	↑	
Calcarine fissure and surrounding cortex				
Cuneus		↑		
Lingual gyrus				
Fusiform gyrus	↑		↑	

Heschl gyrus		↑	↑
Superior temporal gyrus			
Middle temporal gyrus			
Inferior temporal gyrus			
Temporal pole: superior temporal gyrus			↑
Temporal pole: middle temporal gyrus	↑	↑	↑
Parahippocampal gyrus			
Anterior cingulate and paracingulate gyri			
Median cingulate and paracingulate gyri		↑	↑
Posterior cingulate gyrus	↑		↑
Insula			↑
Hippocampus			
<hr/>			
Right Hemisphere			
Gyrus Rectus		↑	↑
Olfactory Cortex		↑	↑
Superior frontal gyrus, orbital part			
Frontal gyrus, medial orbital part			↑
Middle frontal gyrus, orbital part			↑
Inferior frontal gyrus, orbital part		↑	↑
Superior frontal gyrus	↑		↑
Middle frontal gyrus	↑	↑	↑
Inferior frontal gyrus, opercular part			
Inferior frontal gyrus, triangular part			↑
Superior frontal gyrus, medial			↑
Supplementary motor area	↑		↑
Paracentral lobule			
Precentral gyrus			↑
Rolandic operculum			↑
Postcentral gyrus			
Superior parietal gyrus	↑		↑
Inferior parietal, but supramarginal and angular gyri			↑
Supramarginal gyrus			
Angular gyrus		↑	
Precuneus		↑	↑
Superior occipital gyrus		↑	↑
Middle occipital gyrus			



Inferior occipital gyrus	↑	↑
Calcarine fissure and surrounding cortex		↑
Cuneus		
Lingual gyrus		↑
Fusiform gyrus		↑
Heschl gyrus	↑	↑
Superior temporal gyrus		
Middle temporal gyrus		
Inferior temporal gyrus	↑	↑
Temporal pole: superior temporal gyrus		↑
Temporal pole: middle temporal gyrus		
Parahippocampal gyrus	↑	↑
Anterior cingulate and paracingulate gyri	↑	
Median cingulate and paracingulate gyri	↑	↑
Posterior cingulate gyrus	↑	↑
Insula	↑	
Hippocampus		

---

738  
739  
740

**Appendix 1 Table 2.** Regions of interest (ROIs) that manifest significant Eccentricity differences between groups in the theta band.

ROIs	Pairwise Permutation Comparisons (FDR-corrected)			
	Children (N = 24) vs Adults (N = 24)	5 Y.O. (N = 10) vs 10 Y.O. (N = 14)	5 Y.O. (N = 10) vs 10 Y.O. (N = 14)	10 Y.O. (N=14) vs Adults (N=24)
<b>Left Hemisphere</b>				
Gryus Rectus	↑	↑	↑	
Olfactory Cortex	↑		↑	
Superior frontal gyrus, orbital part	↑	↑	↑	
Frontal gyrus, medial orbital part	↑	↑	↑	
Middle frontal gyrus, orbital part	↑	↑	↑	
Inferior frontal gyrus, orbital part	↑	↑	↑	
Superior frontal gyrus	↑	↑	↑	
Middle frontal gyrus	↑		↑	
Inferior frontal gyrus, opercular part		↑	↑	
Inferior frontal gyrus, triangular part	↑	↑	↑	
Superior frontal gyrus, medial	↑		↑	
Supplementary motor area	↑	↑	↑	
Paracentral lobule	↑	↑	↑	
Precentral gyrus	↑	↑	↑	
Rolandic operculum	↑	↑	↑	
Postcentral gyrus	↑	↑	↑	
Superior parietal gyrus	↑	↑	↑	
Inferior parietal, but supramarginal and angular gyri				
Supramarginal gyrus	↑	↑	↑	
Angular gyrus	↑		↑	
Precuneus	↑		↑	
Superior occipital gyrus	↑	↑	↑	
Middle occipital gyrus	↑	↑	↑	↑
Inferior occipital gyrus		↑	↑	
Calcarine fissure and surrounding cortex	↑		↑	↑
Cuneus	↑		↑	
Lingual gyrus		↑	↑	
Fusiform gyrus	↑	↑	↑	↑

Heschl gyrus	↑	↑	↑	
Superior temporal gyrus	↑		↑	
Middle temporal gyrus	↑		↑	↑
Inferior temporal gyrus	↑		↑	
Temporal pole: superior temporal gyrus	↑	↑	↑	
Temporal pole: middle temporal gyrus		↑	↑	
Parahippocampal gyrus	↑	↑	↑	
Anterior cingulate and paracingulate gyri	↑	↑	↑	
Median cingulate and paracingulate gyri			↑	
Posterior cingulate gyrus	↑		↑	↑
Insula		↑	↑	
Hippocampus	↑	↑	↑	
<hr/>				
Right Hemisphere				
Gryus Rectus		↑	↑	
Olfactory Cortex		↑	↑	
Superior frontal gyrus, orbital part	↑	↑	↑	
Frontal gyrus, medial orbital part	↑		↑	
Middle frontal gyrus, orbital part	↑	↑	↑	
Inferior frontal gyrus, orbital part	↑	↑	↑	
Superior frontal gyrus			↑	
Middle frontal gyrus	↑		↑	
Inferior frontal gyrus, opercular part	↑	↑	↑	
Inferior frontal gyrus, triangular part	↑	↑	↑	
Superior frontal gyrus, medial	↑	↑	↑	↑
Supplementary motor area	↑	↑	↑	↑
Paracentral lobule	↑	↑	↑	↑
Precentral gyrus	↑	↑	↑	
Rolandic operculum	↑		↑	
Postcentral gyrus	↑	↑	↑	
Superior parietal gyrus	↑		↑	
Inferior parietal, but supramarginal and angular gyri	↑	↑	↑	
Supramarginal gyrus	↑	↑	↑	
Angular gyrus	↑	↑	↑	
Precuneus	↑		↑	
Superior occipital gyrus	↑		↑	
Middle occipital gyrus	↑		↑	

Inferior occipital gyrus	↑		↑	↑
Calcarine fissure and surrounding cortex	↑		↑	
Cuneus	↑		↑	
Lingual gyrus	↑	↑	↑	
Fusiform gyrus	↑		↑	
Heschl gyrus	↑	↑	↑	
Superior temporal gyrus		↑	↑	
Middle temporal gyrus	↑		↑	
Inferior temporal gyrus	↑	↑	↑	
Temporal pole: superior temporal gyrus	↑	↑	↑	
Temporal pole: middle temporal gyrus	↑	↑	↑	
Parahippocampal gyrus	↑		↑	
Anterior cingulate and paracingulate gyri	↑	↑	↑	
Median cingulate and paracingulate gyri	↑	↑	↑	
Posterior cingulate gyrus	↑	↑	↑	
Insula	↑		↑	↑
Hippocampus	↑	↑	↑	

742  
743  
745

**Appendix 1 Table 3.** Regions of interest (ROIs) that manifest significant Eccentricity differences between groups in the alpha band.

ROIs	Pairwise Permutation Comparisons (FDR-corrected)			
	Children (N = 24) vs Adults (N = 24)	5 Y.O. (N = 10) vs 10 Y.O. (N = 14)	5 Y.O. (N = 10) vs Adults (N = 24)	10 Y.O. (N=14) vs Adults (N=24)
<b>Left Hemisphere</b>				
Gryus Rectus			↑	
Olfactory Cortex			↑	
Superior frontal gyrus, orbital part				
Frontal gyrus, medial orbital part	↑		↑	
Middle frontal gyrus, orbital part		↑	↑	
Inferior frontal gyrus, orbital part	↑	↑	↑	
Superior frontal gyrus				↑
Middle frontal gyrus	↑		↑	
Inferior frontal gyrus, opercular part	↑		↑	
Inferior frontal gyrus, triangular part	↑	↑	↑	
Superior frontal gyrus, medial	↑		↑	
Supplementary motor area	↑		↑	
Paracentral lobule	↑	↑	↑	
Precentral gyrus	↑		↑	
Rolandic operculum	↑	↑	↑	
Postcentral gyrus	↑		↑	
Superior parietal gyrus	↑		↑	
Inferior parietal, but supramarginal and angular gyri	↑		↑	
Supramarginal gyrus		↑	↑	
Angular gyrus	↑		↑	
Precuneus	↑		↑	
Superior occipital gyrus	↑	↑	↑	
Middle occipital gyrus	↑	↑	↑	
Inferior occipital gyrus	↑		↑	
Calcarine fissure and surrounding cortex	↑	↑	↑	
Cuneus	↑		↑	
Lingual gyrus	↑	↑	↑	
Fusiform gyrus	↑		↑	↑



Heschl gyrus	↑		↑	
Superior temporal gyrus	↑		↑	
Middle temporal gyrus	↑	↑	↑	
Inferior temporal gyrus	↑		↑	↑
Temporal pole: superior temporal gyrus	↑	↑	↑	
Temporal pole: middle temporal gyrus	↑		↑	
Parahippocampal gyrus	↑		↑	
Anterior cingulate and paracingulate gyri			↑	
Median cingulate and paracingulate gyri	↑		↑	↑
Posterior cingulate gyrus	↑		↑	↑
Insula	↑		↑	
Hippocampus				
<hr/>				
Right Hemisphere				
Gryus Rectus	↑		↑	
Olfactory Cortex	↑		↑	
Superior frontal gyrus, orbital part	↑	↑	↑	
Frontal gyrus, medial orbital part			↑	
Middle frontal gyrus, orbital part		↑	↑	
Inferior frontal gyrus, orbital part		↑	↑	
Superior frontal gyrus	↑		↑	
Middle frontal gyrus	↑	↑	↑	
Inferior frontal gyrus, opercular part	↑		↑	
Inferior frontal gyrus, triangular part	↑	↑	↑	
Superior frontal gyrus, medial	↑	↑	↑	
Supplementary motor area	↑		↑	↑
Paracentral lobule	↑		↑	↑
Precentral gyrus	↑		↑	
Rolandic operculum				
Postcentral gyrus	↑		↑	
Superior parietal gyrus	↑	↑	↑	
Inferior parietal, but supramarginal and angular gyri	↑		↑	
Supramarginal gyrus				
Angular gyrus			↑	
Precuneus	↑		↑	↑
Superior occipital gyrus			↑	
Middle occipital gyrus			↑	

Inferior occipital gyrus	↑		↑	
Calcarine fissure and surrounding cortex	↑		↑	
Cuneus		↑	↑	
Lingual gyrus	↑		↑	
Fusiform gyrus			↑	
Heschl gyrus	↑		↑	
Superior temporal gyrus				
Middle temporal gyrus				
Inferior temporal gyrus			↑	
Temporal pole: superior temporal gyrus		↑	↑	
Temporal pole: middle temporal gyrus	↑	↑	↑	
Parahippocampal gyrus	↑	↑	↑	
Anterior cingulate and paracingulate gyri		↑	↑	
Median cingulate and paracingulate gyri	↑		↑	↑
Posterior cingulate gyrus	↑		↑	↑
Insula	↑		↑	
Hippocampus	↑		↑	

746  
747  
748

**Appendix 1 Table 4.** Regions of interest (ROIs) that manifest significant Eccentricity differences between groups in the beta band.

ROIs	Pairwise Permutation Comparisons (FDR-corrected)			
	Children (N = 24) vs Adults (N = 24)	5 Y.O. (N = 10) vs 10 Y.O. (N = 14)	5 Y.O. (N = 10) vs Adults (N = 24)	10 Y.O. (N=14) vs Adults (N=24)
<b>Left Hemisphere</b>				
Gyrus Rectus				
Olfactory Cortex	↑		↑	
Superior frontal gyrus, orbital part	↑		↑	
Frontal gyrus, medial orbital part				
Middle frontal gyrus, orbital part	↑		↑	
Inferior frontal gyrus, orbital part	↑		↑	
Superior frontal gyrus	↑		↑	
Middle frontal gyrus				
Inferior frontal gyrus, opercular part	↑		↑	
Inferior frontal gyrus, triangular part	↑		↑	
Superior frontal gyrus, medial	↑	↑	↑	↑
Supplementary motor area	↑	↑	↑	
Paracentral lobule				
Precentral gyrus	↑		↑	
Rolandic operculum				
Postcentral gyrus			↑	
Superior parietal gyrus				
Inferior parietal, but supramarginal and angular gyri	↑		↑	
Supramarginal gyrus			↑	
Angular gyrus				
Precuneus		↑	↑	
Superior occipital gyrus	↑		↑	
Middle occipital gyrus				
Inferior occipital gyrus			↑	
Calcarine fissure and surrounding cortex				
Cuneus	↑			
Lingual gyrus				
Fusiform gyrus		↑	↑	

Heschl gyrus				
Superior temporal gyrus				
Middle temporal gyrus	↑		↑	
Inferior temporal gyrus	↑		↑	
Temporal pole: superior temporal gyrus	↑		↑	↑
Temporal pole: middle temporal gyrus	↑		↑	↑
Parahippocampal gyrus	↑	↑	↑	
Anterior cingulate and paracingulate gyri	↑		↑	
Median cingulate and paracingulate gyri				
Posterior cingulate gyrus	↑	↑	↑	
Insula			↑	
Hippocampus			↑	
<hr/>				
Right Hemisphere				
Gryus Rectus	↑	↑	↑	
Olfactory Cortex				
Superior frontal gyrus, orbital part	↑		↑	
Frontal gyrus, medial orbital part	↑		↑	
Middle frontal gyrus, orbital part	↑	↑	↑	↑
Inferior frontal gyrus, orbital part	↑		↑	
Superior frontal gyrus				
Middle frontal gyrus	↑		↑	
Inferior frontal gyrus, opercular part	↑		↑	
Inferior frontal gyrus, triangular part	↑		↑	
Superior frontal gyrus, medial	↑	↑	↑	
Supplementary motor area	↑			
Paracentral lobule				
Precentral gyrus		↑	↑	
Rolandic operculum	↑		↑	↑
Postcentral gyrus		↑	↑	
Superior parietal gyrus				
Inferior parietal, but supramarginal and angular gyri				
Supramarginal gyrus			↑	
Angular gyrus	↑		↑	
Precuneus	↑		↑	
Superior occipital gyrus				
Middle occipital gyrus	↑		↑	

Inferior occipital gyrus				
Calcarine fissure and surrounding cortex	↑			
Cuneus				
Lingual gyrus				
Fusiform gyrus	↑		↑	
Heschl gyrus	↑		↑	↑
Superior temporal gyrus			↑	
Middle temporal gyrus		↑	↑	
Inferior temporal gyrus			↑	
Temporal pole: superior temporal gyrus	↑		↑	
Temporal pole: middle temporal gyrus	↑		↑	
Parahippocampal gyrus	↑		↑	
Anterior cingulate and paracingulate gyri	↑		↑	
Median cingulate and paracingulate gyri				
Posterior cingulate gyrus	↑		↑	
Insula	↑	↑	↑	
Hippocampus	↑		↑	



750  
751  
753

**Appendix 1 Table 5.** Regions of interest (ROIs) that manifest significant Eccentricity differences between groups in the low gamma band.

ROIs	Pairwise Permutation Comparisons (FDR-corrected)			
	Children (N = 24) vs Adults (N = 24)	5 Y.O. (N = 10) vs 10 Y.O. (N = 14)	5 Y.O. (N = 10) vs Adults (N = 24)	10 Y.O. (N=14) vs Adults (N=24)
<b>Left Hemisphere</b>				
Gryus Rectus				
Olfactory Cortex				
Superior frontal gyrus, orbital part			↑	
Frontal gyrus, medial orbital part				
Middle frontal gyrus, orbital part		↑	↑	
Inferior frontal gyrus, orbital part	↑	↑	↑	
Superior frontal gyrus				
Middle frontal gyrus	↑		↑	
Inferior frontal gyrus, opercular part	↑		↑	
Inferior frontal gyrus, triangular part				
Superior frontal gyrus, medial				
Supplementary motor area				
Paracentral lobule	↑			
Precentral gyrus	↑		↑	
Rolandic operculum				
Postcentral gyrus				
Superior parietal gyrus				
Inferior parietal, but supramarginal and angular gyri				
Supramarginal gyrus		↑	↑	
Angular gyrus	↑		↑	
Precuneus	↑		↑	
Superior occipital gyrus	↑		↑	
Middle occipital gyrus	↑		↑	↑
Inferior occipital gyrus	↑			
Calcarine fissure and surrounding cortex			↑	
Cuneus	↑		↑	↑
Lingual gyrus				
Fusiform gyrus				

Heschl gyrus			↑
Superior temporal gyrus	↑	↑	↑
Middle temporal gyrus			
Inferior temporal gyrus			
Temporal pole: superior temporal gyrus	↑		↑
Temporal pole: middle temporal gyrus			
Parahippocampal gyrus			
Anterior cingulate and paracingulate gyri			
Median cingulate and paracingulate gyri	↑		↑
Posterior cingulate gyrus	↑		↑
Insula	↑		
Hippocampus			
<hr/>			
Right Hemisphere			
Gyrus Rectus		↑	↑
Olfactory Cortex			
Superior frontal gyrus, orbital part			↑
Frontal gyrus, medial orbital part	↑		↑
Middle frontal gyrus, orbital part	↑	↑	↑
Inferior frontal gyrus, orbital part	↑		↑
Superior frontal gyrus			
Middle frontal gyrus			
Inferior frontal gyrus, opercular part			
Inferior frontal gyrus, triangular part			
Superior frontal gyrus, medial	↑	↑	↑
Supplementary motor area			
Paracentral lobule	↑		↑
Precentral gyrus	↑		↑
Rolandic operculum			↑
Postcentral gyrus			
Superior parietal gyrus			
Inferior parietal, but supramarginal and angular gyri			
Supramarginal gyrus	↑		↑
Angular gyrus			↑
Precuneus			
Superior occipital gyrus			
Middle occipital gyrus	↑		↑

Inferior occipital gyrus			
Calcarine fissure and surrounding cortex	↑		↑
Cuneus	↑		↑
Lingual gyrus			
Fusiform gyrus			↑
Heschl gyrus			
Superior temporal gyrus			
Middle temporal gyrus			↑
Inferior temporal gyrus			↑
Temporal pole: superior temporal gyrus			↑
Temporal pole: middle temporal gyrus	↑	↑	↑
Parahippocampal gyrus			
Anterior cingulate and paracingulate gyri			↑
Median cingulate and paracingulate gyri			
Posterior cingulate gyrus	↑		↑
Insula			↑
Hippocampus	↑		↑

754